Novel correlative adaptation between Rubisco and CO_2 concentrating mechanisms in seagrasses

Sebastià Capó-Bauçà[1], Concepción Iñiguez[1*], Pere Aguiló-Nicolau[1] and Jeroni Galmés[1]

[1]Research Group on Plant Biology under Mediterranean Conditions, Universitat de les Illes Balears–INAGEA, Palma, Balearic Islands

*Author for correspondence:

Concepción Iñiguez

Tel: +34971259720; Fax: +34971173168;

E-mail: c.iniguez@uib.es

Research Group on Plant Biology under Mediterranean Conditions. Universitat de les Illes Balears, Ctra. Valldemossa km. 7.5; 07122 Palma, Balearic Islands

Abstract

Submerged angiosperms sustain some of the most productive and diverse ecosystems worldwide. However, their carbon acquisition and assimilation mechanisms remain poorly explored, missing an important step in the evolution of photosynthesis during the colonization of aquatic environments by angiosperms. Here, we reveal a convergent Rubisco kinetic adaptation in phylogenetically distant seagrass species that shared catalytic efficiencies and CO_2 and O_2 affinities up to 3-times lower than those observed in phylogenetically closer angiosperms from terrestrial, freshwater and brackish water habitats. This Rubisco kinetic convergence was found to correlate with the effectiveness of seagrass CO_2 concentrating mechanisms (CCMs), which likely evolved in response to the constant CO_2 limitation in marine environments. The observed Rubisco kinetic adaptation in seagrasses more closely resembles that seen in eukaryotic algae operating CCMs rather than that reported in terrestrial C_4 plants. Thus, our results demonstrate a general pattern of co-evolution between Rubisco function and biophysical CCM effectiveness that traverses across distantly related aquatic lineages.

Keywords: Aquatic plants, CO_2 concentrating mechanisms, CO_2-fixation, freshwater angiosperms, photosynthesis, *rbc*L, Rubisco kinetics, seagrasses.

Main text

The colonization of freshwater, brackish water and marine coastal ecosystems by angiosperms has proven crucial in the sequestration of carbon, nutrient cycling and erosion protection of aquatic environments[1,2]. Such key ecological roles have necessitated extensive physiological adaptation in response to profound changes in the availability of light, nutrients and in the rates of gas exchange. In terms of photosynthetic carbon assimilation, gas exchange in the aquatic environment refers to both gas diffusion and CO_2 availability. CO_2 diffusion in water is ~10,000 times slower than in air[3], and consequently the boundary layer of submerged plant leaves can provoke a severe limitation in the uptake and supply of CO_2 to the carbon fixing enzyme Ribulose-1,5-biphosphate (RuBP) carboxylase oxygenase (Rubisco). The associated slower diffusion of O_2 in water also impairs its release from the leaves, leading to higher rates of competitive RuBP oxygenation by Rubisco, and consequently, increased energy consuming and CO_2-releasing by the photorespiration process[4].

Limitations to CO_2 availability for photosynthesis in submerged plants are especially critical under increasing temperature and salinity, since both CO_2 and O_2 solubilities decrease[5]. In solution, the dissolved inorganic carbon (DIC) can exist as either CO_2, bicarbonate (HCO_3^-) or carbonate (CO_3^{2-}) ions whose equilibrium varies with temperature, salinity (ionic strength), alkalinity and pH[6]. At a basic pH of ~8-8.5, the dominant form of DIC is HCO_3^-, with CO_2 present at less than 1% of the total DIC[7]. Consequently, CO_2 availability for aquatic photosynthesis is limited by both the slow gaseous diffusion and the physiochemistry of the water at air-equilibrium conditions.

Moreover, in aquatic environments, there can be a wide deviation from the equilibrium among the DIC forms caused by biological activity, encountering periods of CO_2 oversaturation during the night and intermittent events of CO_2 depletion during the

74 day[8]. The deviation from air-equilibrium conditions occurs when the interconversion
75 between CO_2 and HCO_3^- is slower than the photosynthetic CO_2 fixation or CO_2 release
76 during respiration (in absence of enzyme catalysis, i.e., carbonic anhydrase). Additional
77 CO_2 input from root respiration in groundwater, and oxidation of organic matter from the
78 catchment, could also increase CO_2 concentrations in fresh and brackish aquatic
79 environments. The amplitude of the CO_2 fluctuation depends on the buffering capacity of
80 the water, which is determined by water alkalinity. Alkalinity strongly varies in fresh and
81 brackish aquatic environments depending on the catchment composition, and, therefore,
82 a wide fluctuation of CO_2 concentrations can be found in these environments[9], in contrast
83 to the nearly constant alkalinity found in marine environments (~2300 mequivalents m^{-3}).
84 Therefore, the more stable physicochemistry, along with lower solubility of gases and
85 diffusion rates cause a constant CO_2 limitation in seawater. In this sense, the selection of
86 representative plants from different aquatic environments, namely freshwater, brackish
87 water and seawater, is required to assess the carbon acquisition and assimilation
88 adaptations developed by submerged angiosperms. In addition, the closest terrestrial
89 relatives of submerged angiosperms need to be also carefully investigated to avoid
90 possible phylogenetical constrictions in the lineage of aquatic plants.

91 In coping with the CO_2 limitation for photosynthesis, many aquatic photosynthetic
92 organisms have acquired CO_2 concentrating mechanisms (CCMs) throughout their
93 evolution[10]. Despite some evidence of C_4 or CAM-type metabolisms (see Beer et al.[11] and
94 Raven et al.[12]), CCMs in aquatic photosynthetic organisms are mainly based in indirect
95 or direct bicarbonate utilization (known as biophysical CCMs), but up to date, only few
96 indirect physiological evidences of CCMs in submerged angiosperms have been
97 reported[13,14]. These studies partially demonstrated the ability of submerged angiosperms
98 to use HCO_3^- as a source of DIC for photosynthesis, but not the effectiveness of their

CCMs to concentrate CO_2 around Rubisco active sites. Since marine autotrophs might experience a more permanent CO_2 limitation than fresh and brackish water autotrophs, it can be hypothesized that the effectiveness of their CCMs may largely depend on the type of aquatic environment. Such capacity for concentrating CO_2 over environmental CO_2 levels can only be detected by the comparison of photosynthetic *in vivo* and Rubisco *in vitro* carboxylation under ambient O_2[15]. Still, Rubisco kinetic traits in submerged angiosperms have not yet been explored, and their Rubisco affinity for CO_2 is assumed to be as high as in terrestrial C_3 plants[14].

The existence of CCMs, which provoke a significant increase in CO_2 concentration and CO_2/O_2 ratio around Rubisco, generally correlates with a Rubisco catalytic adaptation to this intrachloroplastic environment. For example, near-saturating CO_2 conditions around Rubisco relax the selection pressure for higher Rubisco CO_2 affinity (i.e. higher K_m for CO_2, K_c), allowing the selection for higher carboxylation rates (k_{cat}^c)[16,17]. This is observed in terrestrial plants expressing biochemical CCMs (C_4 and some CAM metabolisms), when compared with terrestrial C_3 plants. When examining Rubisco evolutionary traits, the mechanistic trade-off between K_c and k_{cat}^c should be accounted[18,19]. Although largely corroborated in terrestrial plants[20,21], algae operating biophysical CCMs behave as outliers in these trade-offs[21–25], even within the green lineage (form IB Rubiscos). This scattered behavior may suggest divergent evolutionary trajectories of aquatic Rubiscos in comparison with those from terrestrial plants[21], and may reveal convergent trends among phylogenetically distant organisms inhabiting aquatic environments.

In the present study, we undertook a detailed analysis of the Rubisco kinetic traits and diversity and effectiveness of CCMs (when present) in an array of marine (*Cymodocea nodosa*, *Posidonia oceanica*, *Zostera noltii* and *Zostera marina*), brackish

124 water (*Stuckenia pectinata* and *Ruppia cirrhosa*), freshwater (*Ceratophyllum demersum*
125 and *Vallisneria gigantea*) and terrestrial (*Alisma lanceolatum* and *Triglochin maritima*)
126 angiosperms. These species were selected according to the phylogenetic diversity of
127 fully-submerged angiosperms from the order Alismatales (except for *C. demersum* which
128 is a basal freshwater angiosperm, see Supplementary Fig. 1), being closely-related species
129 from different aquatic environments (freshwater, brackish water and marine). The
130 inclusion of terrestrial species that are phylogenetically situated in between the analyzed
131 aquatic species (Supplementary Fig. 1) was done to further assess the presence/absence
132 of Rubisco kinetic phylogenetic constrictions within the Alismatales plant lineage.

133 Our results reveal an evolutionary adaptation of submerged angiosperm Rubisco
134 kinetics in response to the effectiveness of their biophysical CCMs, indicating that
135 Rubisco adaptations in submerged angiosperms are mostly driven by environmental
136 rather than phylogenetic constraints. Notably, the kinetic properties of seagrass Rubisco
137 were found to significantly diverge from the kinetic trade-off between CO_2 affinity and
138 carboxylation turnover rate shared among terrestrial plants, tending more to resemble that
139 observed in eukaryotic algae operating CCMs. This provides a new insight into the
140 Rubisco and CCM co-evolution in angiosperms.

141

142 *Aquatic environment determines the type of CCMs in angiosperms*

143 The presence and diversity of CCMs were determined in the selected submerged
144 angiosperms using different indirect proxies, as the photosynthetic rate reduction by
145 different CCM inhibitors, pH drift assays and the carbon isotopic discrimination of the
146 leaf biomass, in order to determine if there is an adaptation of carbon utilization
147 mechanisms to the different aquatic environments.

148 The net photosynthetic rate in the submersed leaves of the analyzed aquatic plants
149 decreased 30-55% under the presence of extracellular carbonic anhydrases (CAs)
150 inhibitor, demonstrating the important role of extracellular CAs on the utilization of DIC
151 in these species. The additional inhibition of intracellular CAs significantly reduced the
152 net photosynthetic rate in all species, except in *R. cirrhosa*, *P. oceanica* and *C. nodosa*.
153 Notably, the strongest reduction in net photosynthesis after the inhibition of intracellular
154 CAs (20-30% additionally to the extracellular CA inhibition) was observed in freshwater
155 species (Fig. 1*a* and *b*). In turn, Tris buffer inhibited net photosynthetic rate in all species
156 with the exception of freshwater species (Fig. 1*c*), dismissing a CCM associated with an
157 abaxial acidity and adaxial alkalinity in the leaves of the latter[26,27]. Direct HCO_3^-
158 incorporation by anion-exchange transporters inhibited by 4,4'-diisothiocyanatostilbene-
159 2,2'-disulfonate (DIDS) was irrelevant for photosynthesis in most of the analyzed species,
160 especially in seagrasses (Fig. 1d, Supplementary Table 1), as previously indicated by
161 others[28]. Only *C. demersum* and *S. pectinata* showed a significant photosynthetic
162 inhibition by DIDS (about 20% inhibition of net photosynthesis rate). Our results point
163 out that freshwater species seems to rely mostly on CO_2 diffusion facilitated by
164 extracellular and intracellular carbonic anhydrases (CAs) with a minor contribution of
165 anion-exchange HCO_3^- transporters, contrarily to seagrasses and brackish water species,
166 in which DIC acquisition was mostly mediated by the acidification of the periplasmic
167 space with the assistance of extracellular CAs. The operation of ATPase-mediated HCO_3^-
168 transporters cannot be discarded in seagrasses, due to the specificity of DIDS to anion-
169 exchange transporters (chloride channels).

170 The pH drift assays demonstrated the potential capacity to use HCO_3^- as a source
171 of DIC for photosynthesis in all aquatic species analyzed, as all pH compensation points
172 were above the pH value consistent with diffusive CO_2 entry (Fig. 1e). However, biomass

carbon isotopic discrimination values ($\delta^{13}C$) in the submerged angiosperms, corrected by the carbon isotope composition of the DIC source, suggested a predominant use of HCO_3^- for photosynthesis in seagrasses (-13.2 ± 0.5 ‰) as compared to freshwater species (-23.3 ± 0.9 ‰) (Fig. 1f), assuming similar growth rates and similar intrinsic ^{13}C discrimination of Rubisco for all the analyzed species[29]. It is important to consider that, unlike C_4 metabolism, the expression of biophysical CCMs is facultative, and it is regulated by a large number of environmental factors[10]. This might explain the differences found between the high potential capacity to use HCO_3^- for photosynthesis (determined by long pH drift assays at saturating irradiance) and the actual reduced HCO_3^- use during the growth of the leaf shown by $\delta^{13}C$ values in the freshwater species. Values of $\delta^{13}C$ about -30‰ in the terrestrial species *Alisma lanceolatum* and *T. maritima* demonstrated their C_3 photosynthetic pathway and the absence of an operating CCMs (Supplementary Table 1). Additionally, no significant changes in the net photosynthetic rate were observed in a water pH range of 7-9 in the seagrasses *C. nodosa* or *Z. noltii* (Extended Data Fig. 1), indicating that these species possess an especially strong capacity to use bicarbonate for photosynthesis.

After performing a principal component analysis including all the different CCM proxies measured in aquatic plants, the species were clustered according to their aquatic environment (Extended Data Fig. 2). This integrative assessment supports the hypothesis that differences in the physiochemical properties of the species' habitats impacted the mechanisms of DIC acquisition they have evolved.

Other environmental factors such as N availability can also influence CCMs[10]. In fact, significant positive correlations were found between the maximum photosynthetic rate ($A_{n\ max}$) and either N content (P-value < 0.01 and $R^2 = 0.64$), total soluble protein (TSP, P-value < 0.001 and $R^2 = 0.78$) or Rubisco content (P-value < 0.001 and $R^2 = 0.97$),

198 in line with previous observations in other angiosperms[30,31]. According to literature,
199 CCMs in C_4 angiosperms increase the rate of CO_2 fixed per unit of Rubisco[32], reducing
200 the Rubisco content and, therefore, enhancing their N use efficiency. However, despite a
201 lower Rubisco content in seagrasses (~ 4% of TSP) relative to their terrestrial relatives (~
202 17% of TSP) (Supplementary Table 2), seagrasses did not evolve into higher k_{cat}^c values
203 than their terrestrial relatives (Table 1), compromising potential improvements in N use
204 efficiency, and thus, rejecting the idea that CCMs might evolved in seagrasses in response
205 to low N availability. In fact, recent findings have shown that seagrasses such as *P.*
206 *oceanica* possess terrestrial-type nitrogen-fixing symbiosis with marine bacteria, which
207 enables highly productive seagrass meadows to thrive in nitrogen-limited coastal
208 ecosystems[33].

209

210 *Rubisco catalysis converges in submerged angiosperms sharing environment*

211 Similar Rubisco CO_2/O_2 specificity ($S_{c/o}$) values were found for most of the species
212 analyzed, except for the Rubisco of *Posidonia oceanica* and *Cymodocea nodosa*, showing
213 the highest values (91.0 ± 1.3 and 90.4 ± 1.0 mol mol^{-1}, respectively), and for the Rubisco
214 of *Triglochin maritima* and *Zostera noltii*, showing the lowest values (79.3 ± 1.8 and 72.8
215 ± 1.2 mol mol^{-1}, respectively; Table 1). $S_{c/o}$ obtained for the Rubiscos of the analyzed
216 plants fitted with those previously reported for angiosperms (Fig. 2a). On the contrary,
217 the values for the Michaelis–Menten constants for CO_2 (K_c) and O_2 (K_o) were related to
218 the environment of each species (Table 1). Seagrass Rubiscos presented the highest values
219 for both K_c (between 25.3 and 35.1 μM) and K_o (851.9 – 1328.2 μM), which ranged
220 among the highest values ever reported for angiosperm Rubiscos (Fig. 2b, c). Notably,
221 some seagrass Rubiscos tend to deviate from the general correlation between K_c and K_o
222 (Fig. 2d), showing a higher K_o/K_c ratio.

Despite the high K_c shared among the seagrass Rubiscos, their k_{cat}^c remained relatively low (2.17 – 2.80 s^{-1} Table 1), resulting in much lower carboxylation efficiencies (k_{cat}^c/K_c, between 62.5 – 108.8 s^{-1} mM^{-1}) than those of all other angiosperms (Fig. 2e, f). The low carboxylation efficiency of seagrass Rubiscos was also observed under ambient O_2 (k_{cat}^c/K_c^{air}, Table 1). Accordingly, Rubisco from seagrasses deviated from the mechanistic trade-off between k_{cat}^c and either K_c or K_c^{air} commonly observed among Rubiscos from terrestrial angiosperms, being more closely correlated with the trade-off derived by Iñiguez et al.[21] for Rubisco from non-green algae (Fig. 2g). This fact demonstrates the singularity of Rubisco kinetic traits in seagrasses within angiosperms and denotes a convergence of Rubisco kinetics among phylogenetically distant organisms inhabiting seawaters. On the other hand, Rubisco kinetics in the terrestrial, freshwater and brackish water angiosperms analyzed in this study fitted within the range of variation observed for terrestrial angiosperms, although a gradually decrease in the affinity for CO_2 and O_2 (i.e., higher K_c and K_o), and in the k_{cat}^c/K_c and k_{cat}^c/K_c^{air} ratios was found in the Rubiscos from terrestrial to freshwater and, finally, brackish water species (Fig. 2. and Table 1).

The phylogenetic analysis among submerged and terrestrial angiosperms of the order Alismatales revealed that the submerged plants do not cluster together within the same branch (Supplementary Fig. 1), indicative of a polyphyletic origin of aquatic angiosperms[34,35]. No specific residues of the Rubisco large subunit sequences (*rbc*L) were associated with the adaptation of Rubisco to different aquatic environments, as demonstrated with the lack of positive selection of *rbc*L in the branches of the phylogenetic tree leading to the different species of seagrasses (Supplementary Fig. 1a). Among the species selected in this study, several amino acid changes were detected in the Rubisco large subunit sequences between seagrasses and their closest relatives

(Extended Data Fig. 3a, b). Some of these amino acid changes are located near the active site of Rubisco or in the interface between large and small subunits and could be responsible for the differences observed in the Rubisco kinetics of seagrasses (see Extended Data Fig. 3 and Supplementary Table 3) However, with increasing evidence of the pervasive impact of the Rubisco small subunit (*Rbc*S) on catalysis[36,37], it is also feasible that amino acid differences among the *Rbc*S between the species selected, may be responsible, in part or in full, for the kinetic variation observed.

Overall, the phylogenetic distribution of the species studied did not correlate with the Rubisco kinetic variation (see Supplementary Fig. 1 and Table 1) and supports the hypothesis of Rubisco specialization to the different aquatic environments. This suggests that the Rubisco kinetic variability across aquatic plants stems from adaptation to different CCM physiology rather than a phylogenetic constraint on the *Rbc*L sequence.

Effectiveness of CCMs differs in submerged angiosperms

To determine the capacity of CCMs to concentrate CO_2 near the active site of Rubisco, we compared the *in vitro* Rubisco response to CO_2 under ambient O_2 (*in vitro* CO_2 assimilation) with the *in vivo* photosynthetic response to CO_2 (*in vivo* CO_2 assimilation) in the different species (Table 2 and Fig. 3). In seagrasses, the *in vivo* CO_2 assimilation was 40 – 60% higher than the *in vitro* CO_2 assimilation under ambient CO_2 conditions (Fig. 3d), indicating that CO_2 must be concentrated at the Rubisco active sites, in order to sustain the rates of *in vivo* CO_2 assimilation observed in these species. In addition, seagrasses presented the highest photosynthetic affinity for CO_2 (so the lowest $K_{m\ in\ vivo}$, with an average of 7.1 ± 0.7 μM) and DIC (average $K_{m\ in\ vivo\ (DIC)}$ of 0.91 ± 0.07 mM) (Table 2). On the contrary, the *in vivo* CO_2 assimilation was lower than the *in vitro* CO_2 assimilation in the freshwater species under ambient CO_2 conditions (Fig. 3b), suggesting

mesophyll diffusive limitation to the acquisition of CO_2 in these plants. Regarding the brackish water and terrestrial species, similar *in vitro* and *in vivo* CO_2 assimilation rates were observed within each group (Fig. 3a and c).

The ratio between the *in vitro* Rubisco semi-saturation constant for CO_2 under ambient O_2 (K_c^{air}) and the *in vivo* photosynthetic semi-saturation constant for CO_2 ($K_{m\ in\ vivo}$), $K_c^{air}/K_{m\ in\ vivo}$, can be used to infer the fold-change that environmental CO_2 is concentrated or reduced near the Rubisco active site to sustain the observed photosynthetic rates *in vivo*[38]. In this sense, the environmental CO_2 concentration can decrease 2 - 2.5 times along the diffusion pathway from the bulk medium to Rubisco active sites[15], due to restrictions in CO_2 diffusion imposed by the permeability of the cell wall, lipidic membranes and diffusion boundary layers. Hence, to confirm an effective CO_2 concentrating mechanism around Rubisco, a $K_c^{air}/K_{m\ in\ vivo}$ ratio above 2.5 is required[15]. Among the studied species, only seagrasses presented a $K_c^{air}/K_{m\ in\ vivo}$ ratio above 2.5, with an average of 6, indicative of their higher effectiveness to concentrate CO_2, whereas for brackish water species the capacity to concentrate CO_2 around Rubisco over environmental CO_2 levels cannot be confirmed (average $K_c^{air}/K_{m\ in\ vivo}$ ratio of 1.5). Freshwater and terrestrial species showed an average $K_c^{air}/K_{m\ in\ vivo}$ ratio below 1 (0.32 and 0.50 respectively) indicating the absence of CO_2 concentrating capacity at Rubisco active sites during steady-state photosynthesis.

Rubisco kinetics and CCMs co-evolved in submerged angiosperms

When modelling the Rubisco potential for CO_2 assimilation (A_{Rub}) over different CO_2 concentrations, seagrasses showed lower A_{Rub} than brackish and freshwater species for the whole range of CO_2 concentrations tested (Fig. 4 and Extended Data Fig. 4). Brackish water species also presented lower A_{Rub} than freshwater species, denoting that A_{Rub} is

lower in species with higher effectiveness to concentrate CO_2. Nevertheless, the ratio between A_{Rub} of either brackish water plants or seagrasses, and A_{Rub} of freshwater plants, increased with the rise in CO_2 concentration (Fig. 4). This fact is indicative of an adaptation of Rubisco kinetic traits to higher chloroplastic CO_2 concentrations, and supports the occurrence of co-evolution between CO_2 concentration effectiveness and Rubisco CO_2 assimilation, as previously proposed in other species expressing CCMs[21,23,39,40].

To determine the limitation exerted by Rubisco activity to the leaf net CO_2 assimilation rate in the species analyzed, the biochemical model of Farquhar et al.[41] was used. On average, modelled leaf net CO_2 assimilation rate ($A_{n\ modelled}$) for seagrasses was limited by Rubisco activity up to a chloroplast CO_2 concentration (C_c) of 32 μM, compared to the 24, 19 and 9 μM of brackish water, freshwater and terrestrial species, respectively (Fig. 5). However, as seagrasses presented the highest CO_2 concentration effectiveness, the $A_{n\ modelled}$ of seagrasses ceased to be limited by Rubisco activity at the lowest extracellular CO_2 concentration ($C_a \sim 5$ μM). These results suggest that, under the C_a found in the marine environment (see Supplementary Table 4), and assuming a constant J_{max}/V_{max}^c of 2 (J_{max}, maximum capacity of electron transport rate; V_{max}^c, maximum velocity of carboxylation), photosynthesis in seagrasses may be limited by the thylakoid-based reactions (activity of photosystems, chloroplastic electron transport chain and ATP-ases) required to regenerate the ribulose bisphosphate (RuBP) rather than by Rubisco carboxylation (Extended Data Fig. 5). Further investigation is needed for a better understanding of the interplay between RuBP regeneration and Rubisco activity in submerged angiosperms, specially to review the assumptions made in the present study of a constant J_{max}/V_{max}^c of 2 (see the methods section).

Discussion

The knowledge about the mechanisms driving carbon acquisition and assimilation in submerged angiosperms represents a key step in the comprehension of the photosynthetic evolution during angiosperm water colonization. Here, we demonstrated an evolutionary adaptation of Rubisco kinetics to the type and effectiveness of biophysical CCMs expressed in submerged angiosperms from marine, brackish water and freshwater environments. The mechanistic trade-offs between Rubisco kinetics previously described for terrestrial plants were eluded by seagrasses, tending to resemble more those observed for eukaryotic algae operating CCMs and suggesting a general pattern of coevolution across marine photosynthetic organisms.

Our results highlight that CCMs are determined by the aquatic environment of the species (Fig. 1, 3 and Extended Data Fig. 1). The low CO_2 levels in seawater (14 – 18 µM of CO_2) relative to higher, more variable levels, in freshwater and brackish water environments (7 – 250 and 0 – 931 µM of CO_2, respectively, Supplementary Table 4) might have led to the evolution of more effective CCMs in seagrasses (Fig. 3), that seems to comprise a higher activity of extrusion proton pumps and extracellular carbonic anhydrases (Fig. 1), as previously observed[34]. Moreover, the highly effective CCMs in seagrasses could also be related with the presence of transfer cells-like structures in their epidermis[14]. In turn, freshwater species seem to rely mainly on diffusive entry of CO_2, with a minor contribution of anion-exchange HCO_3^- transporters, suggesting that inputs of CO_2 from the catchment could be the major carbon source[42]. Nevertheless, the facultative expression of more effective CCMs under depleted CO_2 conditions cannot be discarded in freshwater plants, as the diffusion limitation impaired by the boundary layer and biological membranes would reduce CO_2 concentration below the CO_2 compensation point for Rubisco[15].

The effectiveness of CCMs to concentrate CO_2 near Rubisco differentially influenced its kinetic adaptation in submerged plants (Table 1). The CO_2 concentration around Rubisco has been suggested as a selection pressure for Rubisco kinetics[43]. In C_4 plants, the high CO_2 concentration near the active sites of Rubisco provided by the CCMs promoted the evolution towards a higher k_{cat}^c at expenses of a reduction in the affinity of Rubisco for CO_2 (higher K_c)[44]. However, this trade-off between k_{cat}^c and K_c is scattered when photosynthetic organisms with biophysical CCMs are considered[21]. Our analysis demonstrates a co-evolution of the Rubisco affinity for CO_2 and the biophysical CCMs in submerged angiosperms, in line with previous reports for different phylogenetic groups of algae[21,23–25]. Contrarily to plants with biochemical CCMs (C_4 and some CAM plants), the reduction in the affinity for CO_2 was not accompanied by a proportionally increase in k_{cat}^c in the Rubiscos of submerged angiosperms (Fig. 2). Instead, a severe reduction in k_{cat}^c/K_c was observed in the species with more effective biophysical CCMs (seagrasses), leading to k_{cat}^c/K_c values that place outside the natural range previously reported for angiosperms, and within the range reported for marine algae with biophysical CCMs (Fig. 2). Other green eukaryotic algae possessing very effective biophysical CCMs from terrestrial/freshwater environments also showed Rubiscos with low k_{cat}^c/K_c values[22,23], indicative that biophysical CCMs are one of the main drivers of Rubisco evolution in aquatic organisms.

Not only the effectiveness of CCMs may relax the selection pressure for higher k_{cat}^c/K_c, but also the extent of time that a CCM has been operating throughout the evolution[16]. Seagrasses families separated from their terrestrial ancestors about 100 Ma and diversified in the past 70 Ma[45,46] (Supplementary Fig. 1a). Despite higher atmospheric CO_2 concentrations reported for this period[47], seagrass ancestors probably had already developed biophysical CCMs that allowed them to overcome the low CO_2 diffusion in

seawater. This suggests a coexistence of Rubisco and CCMs in seagrass ancestors before the drop in the environmental CO_2 30 Ma ago. This environmental CO_2 drop likely led to the evolution of CCMs in C_4 lineages[48] and to the improvement of k_{cat}^c/K_c in the Rubisco of C_3 plants[16]. As a result, the long-extended time of co-evolution of Rubisco with biophysical CCMs could have relaxed the selection towards higher k_{cat}^c/K_c values in seagrass Rubiscos.

On the other hand, a recent diversification of families including brackish water and freshwater species was demonstrated in literature (50-20 Ma ago[49–52]). In this sense, the higher values of k_{cat}^c/K_c found for the Rubisco of freshwater and brackish water species could be related with a shorter period of coexistence between Rubisco and CCMs. However, the fossil record indicates that close phylogenetic relatives of the submerged basal angiosperm *C. demersum* inhabited freshwater environments 100 Ma ago[42,53], and therefore the higher values of k_{cat}^c/K_c found in the Rubisco of freshwater species might probably be promoted by a less effective CCMs.

Recently, Bouvier et al.[54] showed that Rubisco kinetic adaptation in terrestrial C_3 plants are more constricted by their phylogeny rather than by Rubisco catalytic trade-offs. According to this, the low values of k_{cat}^c/K_c and k_{cat}^c/K_c^{air} in seagrass Rubiscos could also be related with a phylogenetic signal of their plant lineage. However, the higher k_{cat}^c/K_c and k_{cat}^c/K_c^{air} values of Rubiscos from terrestrial and freshwater closest relatives of the different families of seagrasses analyzed (Fig. 2, Table 1) demonstrate a wide Rubisco kinetic diversity in the Alismatales plant lineage that cannot be related with a phylogenetic constraint, reinforcing the premise of evolutionary convergence in seagrass Rubisco kinetics driven by effective CCMs.

The O_2 concentration around Rubisco could be another important driver for Rubisco kinetic traits evolution, especially in aquatic environments[40]. During steady-state

398 photosynthesis, O_2 can be accumulated up to 35% inside seagrass leaves due to lower O_2
399 diffusion in seawater and anatomical diffusive constraints that impede the release of O_2
400 from the leaves[55,56]. Contrary to the main group of C_4 plants, NADP-ME, where most of
401 the photosynthetic O_2 production is spatially separated from CO_2 fixation[57],
402 photosynthetic O_2 production in seagrasses occurs in the proximity of Rubisco active
403 sites[34]. The exceptionally high K_o values found in seagrass Rubiscos (Fig. 2 and Table 1),
404 together with an effective CCM, improve Rubisco functioning under high O_2
405 concentrations[40], which suppose an evolutionary benefit for their photosynthetic
406 performance.

407 Our findings indicate that the catalytic chemistry of Rubisco in seagrasses is on a
408 different adaptive trajectory than in C_3 and C_4 plants, suggesting that the longstanding
409 perception of a mechanically constrained catalysis in angiosperms underpins a bias in the
410 Rubisco kinetic analyses. Moreover, our study reveals a clear example of Rubisco kinetics
411 evolutionary convergence in submerged angiosperms in response to the development and
412 effectiveness of biophysical CCMs, as previously observed for other phylogenetically
413 distant organisms.

414

415 **Materials and Methods**

416 *Plant material*

417 Shoots of *Cymodocea nodosa*, *Posidonia oceanica* and *Zostera noltii* were collected in
418 September-October 2018 from a common meadow located in the Mediterranean Sea,
419 Formentor beach (Pollença, Mallorca, Spain) at 2-3 m depth. *Zostera marina* was
420 obtained from the Atlantic coast at 5 m depth (Pobra do Caramiñal, Coruña, Spain). The
421 freshwater angiosperms *Ceratophyllum demersum* and *Vallisneria gigantea* were

obtained from a local nursery (Fronda, Spain), whereas the brackish water species *Stuckenia pectinata* and *Ruppia cirrhosa* were collected in May 2019 from a coastal lagoon (Parc Natural de s'Albufera, Mallorca, Spain). The terrestrial plant *Alisma lanceolatum* was sampled from Jardí Botanic de Sòller (Mallorca, Spain) and the other terrestrial plant, *Triglochin maritima,* was acquired from Rühlemann's Kräuter & Duftpflanzen (Germany)..

Submerged plants were maintained in an aquarium at 25ºC under continuous aeration in water collected from their respective environments. For most of the species, the average environmental temperature at the day of collection was around 25ºC, except for the Atlantic *Z. marina*. For the latter, the aquarium temperature was gradually increased at a rate of 1ºC per day, from 18ºC up to 23ºC. Water in aquarium was replaced every two days to avoid nutrient depletion. Plants were exposed to a photosynthetically photon flux density (PPFD) similar to the average dose received in their natural environments (50 μmol m^{-2} s^{-1} for *Z. marina*, 100 - 150 μmol m^{-2} s^{-1} for the other seagrasses, and 180 - 200 μmol m^{-2} s^{-1} for freshwater and brackish water species), using LED white light illumination (ELIXIA, Heliospectra, Sweden) with 12:12 h light:dark photoperiod. PPFD was measured inside the water in the middle of the aquarium using a flat mini quantum sensor (LS-C; Walz, Germany) connected to a radiometer (LiCor-250A; Li-Cor Biosciences, USA). Plants of *T. maritima* were maintained in a growth chamber with day:night temperatures of 26 ºC:18 ºC, 50-70 % relative air humidity and PPFD of 300 μmol m^{-2} s^{-1} with a 12 h:12 h light:dark photoperiod, while plants of *A. lanceolatum* were grown in their original environment (gardens of Jardí Botànic de Sóller).

Total dissolved inorganic carbon (DIC) was analyzed in the water collected from the different environments using a total carbon analyser (Multi N/C 2100S. Analytic Jena,

447 Germany). Conductivity and pH were also determined by using a pH meter (Sension+,
448 Hach, USA) and a conductivity meter (Basic30-Crison, Hach, USA). Measured
449 physicochemical characteristics of the different aquatic environments where the plants
450 were collected are reported in Supplementary Table 5.
451

452 *Net photosynthesis, use of inhibitors and effect of pH on submerged angiosperms*

453 Net photosynthesis was determined at 25ºC by O_2 evolution measurements, using Clark
454 type oxygen electrode chambers (Oxygraph, Hansatech, King's Lynn, UK). Electrode
455 chambers were filled with 2 ml of 0.2 µm-filtered water collected from the species
456 respective environments. Leaf pieces of 20-30 mg of fresh weight were exposed to
457 saturating PPFD (600 µmol m^{-2} s^{-1} for seagrasses and 1000 µmol m^{-2} s^{-1} for freshwater
458 and brackish species) provided by white light LED lamps. Saturating PPFD was
459 previously determined for each species by chlorophyll *a* fluorescence light curves using
460 a pulse-amplitude-modulated fluorometer (Dual-PAM-100, Walz, Germany). O_2
461 evolution rates were taken at 3 - 5 min intervals after rate stabilization, using the O2view
462 software (version 2.10, Hansatech, King's Lynn, UK).

463 The role of carbonic anhydrases (CAs) activity in photosynthesis was assessed by
464 measuring the percentage of net photosynthetic rate inhibited under the presence of 200
465 µM azetazolamide (AZ, which inhibits extracellular CAs) and 200 µM 6-ethoxyzolamide
466 (EZ, which inhibits extracellular and intracellular CAs), applied consecutively into the
467 O_2 evolution chamber on the same piece of leaf. The same procedure was followed to
468 measure the percentage of net photosynthetic rate inhibited by 50 mM Tris
469 (hydroxymethyl aminomethane) buffer and by 300 µM of the anion-exchange inhibitor
470 4,4'-diisothiocyanatostilbene-2,2'-disulfonate (DIDS), applied independently into the

chamber using different pieces of leaf. The above reported concentrations of inhibitors represent the final concentrations inside the O_2 evolution chamber.

The same procedure was used to assess the effect of pH on photosynthesis. Net photosynthetic rate was measured at pH 7.5, 8.2 and 9 for seagrasses, and at pH 7, 7.8 and 9.5 for brackish and freshwater species, using the same piece of leaf for the 3 different pH values.

Photosynthesis vs DIC curves in submerged angiosperms

DIC was removed from 0.2 µm filtered-natural water following Invers et al.[58], resulting in < 1 µM of DIC corroborated with a total carbon analyzer (Multi N/C 2100S. Analytic Jena, Germany). After DIC removal, leaf pieces were introduced into the O_2 chamber with 2 ml of DIC-free water from the species respective environment. To prevent O_2 oversaturation during the measure, the initial O_2 concentration in the chamber was reduced to 70 % of the O_2 saturation in air-equilibrated water by bubbling pure nitrogen gas. Oxygen saturation in air-equilibrated water was determined using the software DOTABLES (https://water.usgs.gov/software/DOTABLES/) for the specific salinity of each medium at 25ºC.

After O_2 evolution rate stabilized close to zero, aliquots of a $NaHCO_3$ stock were consecutively added to obtain 8-12 different DIC concentrations into the O_2 chamber (0 - 10 mM for seagrasses species, 0 - 17 mM for brackish water species, and 0 - 20 mM for freshwater species). For each DIC concentration, the oxygen evolution rate was recorded as described above and the dissolved CO_2 concentration was calculated using the CO2sys software[59]. Then, P-C curves were fitted to the Michaelis–Menten function to obtain the DIC-saturated net maximum photosynthetic rate (A_{max}) and the *in vivo* photosynthetic

Michaelis–Menten constant ($K_{m\ in\ vivo}$) for CO_2 and for DIC. A_{max} was normalized by the area of the leaf pieces used in the O_2 chamber, which was measured with the software ImageJ (Wayne Rasband National Institutes of Health, USA).

No pH-buffered water was used for these measurements, as significant inhibitory effect of Tris buffer was detected in all species except for *C. demersum* and *V. gigantea*. In the latter two species, P-C curves were performed with 20 mM Tris pH-buffered water to avoid strong pH variation during the measure. In buffer-sensitive species, the variation of pH was below 0.2 pH units during a complete curve measurement. Although this pH variation could have an small impact on the measure, it is depreciable compared with the inhibitory effect of pH buffers[60,61].

Photosynthesis measurements in terrestrial angiosperms

Gas exchange measurements were performed on terrestrial species using an open infrared gas-exchange analyzer system equipped with a leaf chamber fluorometer (Li-6800, Li-Cor Inc., USA). Measurements were performed on the youngest fully expanded leaves at a leaf temperature of 25ºC and a gas flow of 300 μmol mol^{-1}.

After inducing steady-state photosynthesis at an ambient CO_2 concentration (C_a) of 400 μmol mol^{-1}, photosynthesis responses to varying substomatal CO_2 concentration (A_n–C_i) were measured as explained in Galmés et al.[62] and consisted of 10 measurements per curve (0 to 2000 ppm of C_a). A_n–C_i curves were performed on different individuals at a saturating PPFD of 1200 μmol m^{-2} s^{-1}, determined for each terrestrial species as explained for aquatic plants. Corrections for the CO_2 leakage in and out of the leaf chamber of the Li-6800 were applied to all gas-exchange data, as described by Flexas et al.[63]. A_n–C_i curves were fitted to the Michaelis–Menten equations to obtain the A_{max} and the $K_{m\ in\ vivo}$ for CO_2 as explained above for the P-C curves.

520

521 *pH drift assay*

522 Leaf samples (100-200 mg of FW) were incubated at 25ºC, with continuous saturating
523 white LED light and magnetic stirring, using 7 ml glass vials completely filled with
524 filtered water. The pH was continuously recorded inside the vials (pH electrode Sension+
525 5209, Hach, USA) until the pH was stable at least for one hour. After that, leaf samples
526 were removed and vials were left open to allow re-equilibration with the atmosphere for
527 24 h, and then, pH was measured again to corroborate that no process other than removal
528 of DIC by photosynthesis was altering pH. All assays recovered the initial pH values.

529

530 *Nitrogen content and carbon isotopic discrimination of leaves*

531 The nitrogen leaf concentration and ^{13}C isotopic discrimination was obtained from dried
532 leaf samples as explained in Capó-Bauçà et al.[30]. The ^{13}C isotopic discrimination results
533 are presented as δ vs. PDB. In the submerged plants, the obtained ^{13}C isotopic
534 discrimination of the leaves ($\delta^{13}C_{leaves}$) was corrected with the isotope composition of DIC
535 found in the natural water of the species ($\delta^{13}C_{DIC,}$ Supplementary Table 5), as described
536 by Iñiguez et al.[64].

537

538 *Rubisco catalytic measurements*

539 Between 0.2 - 0.3 g of fresh leaf tissue was sampled under illuminated conditions and
540 frozen immediately in liquid nitrogen. Frozen leaf tissue was homogenized in a pre-
541 chilled mortar with 2 ml of ice-cold extraction buffer consisting of 100 mM Bicine-NaOH
542 (pH 8.1), 20 mM $MgCl_2$, 1 mM ethylenediaminetetraacetic acid (EDTA), 1 mM

benzamidine, 1 mM ε-aminocaproic acid, 10 mM dithiothreitol (DTT), 100 mM β-mercaptoethanol, 2% plant protease inhibitor cocktail (P9599, Merck,, USA), 4 mM phenylmethylsulfonyl fluoride (PMSF), 1 % triton X-100, and either 20 mM of $NaHCO_3$ for seagrasses or 10 mM of $NaHCO_3$ for the freshwater, brackish water and terrestrial species. To avoid oxidation of the extracts, polyvinylpyrrolidone (PVPP) was mixed with the sample at the same weight ratio. The homogenate was centrifuged for 2 min at 15000 x*g* at 4°C and supernatant was used to perform all Rubisco kinetic measurements, except for the Rubisco specificity factor ($S_{c/o}$).

Crude extracts were supplemented with carrier-free $NaH^{14}CO_3$ to adjust the specific radioactivity to 3.7 x 10^{10} Bq mol^{-1} and extracts were preactivated at 25ºC for 20 min in terrestrial, freshwater and brackish water species, and for 10 min in seagrasses for a complete activation of Rubisco, according to preliminary assays. Rates of Rubisco $^{14}CO_2$-fixation were measured at 25°C in 7 ml septum-capped glass scintillation vials as explained in Capó-Bauçà et al.[30]. Each vial contained one of the eight different concentrations of $^{14}CO_2$ ranging from 7 to 170 µM in seagrasses and brackish water species, and from 4 to 120 µM in terrestrial and freshwater species. The Michaelis–Menten constant for CO_2 (K_c) and for O_2 (K_o), and the maximum carboxylase activity (V_{max}^c) was calculated as in Galmés et al.[65]. The Michaelis–Menten constant for O_2 (K_o) were calculated in each biological replicate by a linear fit of K_c measurements obtained under 0% O_2 and under ambient O_2. The carboxylation turnover rate (k_{cat}^c) was calculated by dividing V_{max}^c by the concentration of Rubisco active sites, which was quantified from the same crude protein extracts by 2′-carboxyarabinitol-1,5-bisphosphate (^{14}C-CABP, 130 µM final concentration) binding[66], assuming eight binding sites per Rubisco, and confirmed by SDS-PAGE blots after Coomassie staining, and by immunoblotting using a Rubisco large subunit antibody and purified Rubisco standard (AS01 017S, Agrisera)

568 (Supplementary Fig. 2). The blots were incubated at room temperature for 2.5 h with
569 primary antibody diluted at 1:20000 (AS03 037, Agrisera) and for 1.5 h with secondary
570 antibody diluted at 1:50000 (AS09 602, Agrisera). Total soluble proteins were quantified
571 in the same extracts following the method described by Bradford[67] and using BSA as
572 standard.

573 To confirm that the observed acid-stable ^{14}C was only the result of Rubisco
574 catalytic activity, carboxylation assay controls were carried out at saturating $H^{14}CO_3^-$
575 concentrations either without RuBP addition or using crude extract pre-incubated for 30
576 min with non-radioactive CABP (130 μM). Both controls gave values lower than 1% of
577 the maximum activity in all analyzed species. Concentrations of CO_2 in solution were
578 calculated assuming an acid dissociation constant for carbonic acid (pKa_1) of 6.11 and a
579 solubility constant for CO_2 of 0.034 mol l^{-1} atm^{-1} at 25°C, and using accurate measures
580 of the pH (NBS scale). All described Rubisco kinetic measurements were made using
581 independent crude protein extracts (n=3–6) from different individuals.

582 For $S_{c/o}$, 0.3 - 0.4 g of fresh leaf tissue was homogenized in a pre-chilled mortar
583 with 2 ml of ice-cold extraction buffer containing 100 mM EPPS-NaOH (pH 8.1), 15 mM
584 $MgCl_2$, 1 mM ethylenediaminetetraacetic acid (EDTA), 1 mM benzamidine, 1 mM ε-
585 aminocaproic acid, 10 mM dithiothreitol (DTT), 100 mM β-mercaptoethanol, 2% plant
586 protease inhibitor cocktail (P9599, Merck, USA), 4 mM phenylmethylsulfonyl fluoride
587 (PMSF) and 1 % triton X-100. Then, polyvinylpyrrolidone (PVPP) was mixed with the
588 sample at the same weight ratio. After centrifugation of the homogenate for 2 min at
589 15000 xg at 4°C, the supernatant was passed through a 5-mL Mini-Macroprep High-Q
590 strong anion-exchange cartridge (Bio-Rad, California, USA) following Sharwood et al.[68]
591 and then concentrated ~10 fold using Amicon Ultra 4 (Z740198, Merck, USA). $S_{c/o}$ was
592 analyzed by using [1-^{3}H] RuBP, following the method of Kane et al.[69]. The assay was

593 equilibrated with a gas mixture of 99.95 % O_2 and 0.05% CO_2, and $S_{c/o}$ was calculated
594 using a CO_2/O_2 solubility ratio of 0.038 at 25ºC.

595 As a control, semi-purified extracts of *Z. noltii* and *P. oceanica* which were
596 previously incubated for 30 min with non-radioactive CABP (130 µM), were added at the
597 end of a set of $S_{c/o}$ assays of *T. aestivum*. No changes in $S_{c/o}$ values of *T. aestivum* were
598 detected after 60 min of incubation with CABP-inhibited semi-purified seagrass extracts,
599 dismissing the possibility of further metabolism of the products of *T. aestivum* Rubisco
600 carboxylation and oxygenation by other enzymes present in *Z. noltii* and *P. oceanica*
601 semi-purified extracts.

602

603 *Modelling Rubisco gross assimilation and leaf net CO_2 assimilation rates*

604 Rubisco gross assimilation rate (A_{Rub}) at 25ºC was calculated from the analyzed Rubisco
605 kinetic traits, using the biochemical model of Farquhar et al.[41], as in Galmés et al.[70]. A_{rub}
606 was modelled assuming 1 g Rubisco m^{-2} leaf and at the range of concentrations of CO_2
607 between 100 and 2500 ppm, according to the concentrations expected to be found near
608 Rubisco active sites in the analyzed species.

609 The biochemical model of Farquhar et al.[41] was also used to calculate the leaf net
610 CO_2 assimilation rate ($A_{n\ modelled}$) limited by Rubisco (A_c) and by electron-transport (A_j)
611 for each species and for the different groups of species (average). A constant respiration
612 rate of 0.5 µmol CO_2 m^{-2} s^{-1} in light was assumed. The maximum velocity of
613 carboxylation (V_{max}^c) was calculated by multiplying the concentration of Rubisco active
614 sites measured for each species by their k_{cat}^c. The ratio V_{max}^c/J_{max}, where J_{max} is the
615 maximum capacity of electron transport rate, was assumed to be constant and equal to 2,
616 as commonly reported for angiosperms[71]. To consider the CO_2 concentration capacity of
617 the submerged plants in the model, the ratio $K_c^{air}/K_{m\ in\ vivo}$ was used to transform the CO_2

618 concentration near the Rubisco active sites (C_c) to the corresponding environmental CO_2
619 concentration (C_a). The ratio $K_c^{air}/K_{m\ in\ vivo}$ is an indicative of the strength of CO_2
620 concentration[15], and can be used to infer the times that C_c is concentrated or reduced near
621 the Rubisco active site[38]. Therefore, C_a was calculated using the relationship C_c =
622 $(K_c^{air}/K_{m\ in\ vivo}) \cdot C_a$.

623

624 *Phylogenetic analysis and positive selection of Rubisco large subunit gene (*rbc*L)*

625 A total of 61 species including those representatives from different groups of aquatic
626 angiosperms and close terrestrial relatives were selected to perform a phylogenetic
627 analysis using the Timetree website (http://www.timetree.org/). The Timetree website
628 constructs the phylogenetic relationship of the species and estimates their time of
629 divergence using a standardization and assembly of the data published in literature,
630 following the methodology explained in Hedges et al.[72] and Kumar et al.[73]. The different
631 studies used by the Timetree to perform the phylogenetic tree of Supplementary Fig. 1a
632 are listed in Supplementary Fig. 1b, along with the list of genes used in each publication.

633 Rubisco large subunit nucleotide sequences (*rbcL*) of the 61 species were
634 extracted from the Gene Bank (see accession numbers in Supplementary Fig. 1). The
635 sequences were aligned using ClustalW algorithm and manually adjusted. The final
636 sequence length was 1152 nucleotides in all sequences analyzed, covering more than 80%
637 of the *rbc*L sequence, with the 5' starting at the position 31 and the 3' ending at the
638 position 1182 (*rbc*L *Spinacia oleracea* annotation, accession number NC 002202.1). The
639 sequences of the 10 species selected in the present study (or the most closely related
640 species in the case of *Vallisneria gigantea* and *Alisma lanceolatum*) were
641 phylogenetically reconstructed using maximum likelihood (ML) algorithm with 1000

bootstrap resamplings, using the Tamura 3-parameter model[74]. Initial tree for the heuristic search was obtained automatically by applying neighbour-joining algorithms (NJ and BioNJ) to a matrix of pairwise distances estimated using the Tamura 3 parameter model, and then, selecting the topology with a superior log likelihood value. A discrete Gamma distribution was used to model evolutionary rate differences among sites (5 categories (+G, parameter = 0.1458)). The final tree was represented in Extended Data Fig. 3a. The *rbc*L of the species selected were then translated to an amino acidic sequence. Evolutionary analyses were conducted in MEGA X[75].

The CODEML codon-based package implemented in PAML V4.9[76] was used to detect residues under positive selection in the *rbc*L of the 61 species selected. The ratio of nonsynonymous to synonymous substitution rates (ω) across *rbc*L codons was analyzed using model A as explained by Wissler et al.[45] and Zhang et al.[77]. Two independent analyses were applied, the first using all fully submerged plants as foreground branches, and the second, using only seagrasses as foreground branches (Supplementary Fig. 1a). Posterior probabilities for an amino acid under positive selection ($\omega > 1$) were calculated using the Bayes Empirical Bayes approaches implemented in PAML[77].

Statistical analysis

Significance of differences were tested using one-way analysis of variance (ANOVA), after normality (Anderson-Darling test) and homogeneity of variances (Bartlett test) were confirmed. Post hoc comparisons were performed using Duncan test. Pearson correlation coefficients were obtained for the significance of the association between different variables. P-values lower than 0.05 were considered significant. Data was analyzed using

R (version 3.2.3, 2015-12-10) with Rstudio interphase (RStudio Version 0.99.879 – © 2009-2016, Inc.) and plotted using the ggPlot2 package (ggPlot2 version 2.2.1; Springer-Verlag New York, 2009-2016).

Data availability

All processed data are contained in the manuscript or in the Supplementary Data. The 61 *rbc*L sequences used in this study were extracted from GenBank https://www.ncbi.nlm.nih.gov/nuccore (see accession numbers in Supplementary Figure 1). The reference *rbc*L sequence of *Spinacia oleracea* is under accession number NC 002202.1 in the GenBank. Kinetic data used for Fig. 2 was extracted from Iñiguez et al.[21] (data free available at https://onlinelibrary.wiley.com/doi/10.1111/tpj.14643) and Goudet et al.[23] (data free available at https://nph.onlinelibrary.wiley.com/doi/full/10.1111/nph.16577) Spinach 3D Rubisco structure used in Extended Data Fig. 3 is available at PDB under accession number 1UPM (https://www.rcsb.org/structure/1UPM)

Acknowledgements

This work was financially supported by the Spanish Ministry of Sciences, Innovation and Universities, the Spanish State Research Agency and the European Regional Development Funds (project PGC2018-094621-B-I00) funded to Jeroni Galmés. Sebastià Capó-Bauçà has been supported by an FPU Grant from the Spanish Ministry of Education. Concepción Iñiguez has been supported by a postdoctoral grant from the Government of the Balearic Islands. We thank Trinidad Garcia for technical help and organization of the radioisotope installation at the Serveis Científico-Tècnics (UIB); Drs. Miquel Ribas-Carbó, Cyril Douthe and Biel Martorell for their technical help on the

IRMS; and Jardí Botànic de Sóller, Dr. Maurici Mus, Dr. Antoni Martínez, Dr. Joan Rita, Dr. Xurxo Gago, Dr. Fiona Tomas, Dr. Julia Máñez-Crespo, Dr. Ángel Mateo-Ramírez, Dr. Mateu Fullana and Manuel Del Río Buzón for their help in the identification and sampling of the species. We are grateful to Dr. Xavier Niell and three anonymous reviewers whose comments helped to improve this manuscript.

Author contributions statement

CI and JG conceived and designed the study. SC-B performed the experiments, analyzed the data and produced the figures with help from all authors. PA-N collaborated in the processing of samples. SC-B wrote most of the manuscript with help from all authors.

Competing interests statement

The authors declare no competing interests.

Table 1. Rubisco kinetic parameters. Parameters shown are the Michaelis–Menten constant for CO_2 under 0% O_2 (K_c, n = 5) and under ambient O_2 (K_c^{air}, n = 5), the Michaelis–Menten constant for O_2 (K_o, n = 5); Rubisco CO_2/O_2 specificity ($S_{c/o}$, n = 4), the maximum carboxylation rate (k_{cat}^c, n = 6) and the maximum oxygenation rate (k_{cat}^o, n = 4). Values are means ± s.e. In bold are the mean values for the different environments. Different small letters show significant differences among species (P^1) and capital letters show significant differences among environments (P^2). P^1 and P^2 values were obtained from the F-statistic of one-way ANOVA or from the chi-squared value of Kruskal–Wallis test in the case of non-parametric data. Duncan's test and Kruskal–Wallis test followed by Bonferroni correction for non-parametric data were used to detect differences among means.

Species / environment	$S_{c/o}$ (mol mol^{-1})	K_c (μM)	K_c^{air} (μM)	K_o (μM)	k_{cat}^c (s^{-1})	k_{cat}^o (s^{-1})	k_{cat}^c/K_c (s^{-1} mM^{-1})	k_{cat}^c/K_c^{air} (s^{-1} mM^{-1})	k_{cat}^o/K_o (s^{-1} mM^{-1})
Alisma lanceolatum	81.7 ± 1.3 bc	12.2 ± 0.3 cd	18.9 ± 0.6 cd	463.8 ± 13.3 de	3.42 ± 0.16 ab	1.59 ± 0.09 a	280.6 ± 9.3 ab	180.5 ± 7.4 a	3.43 ± 0.11 b
Triglochin maritima	79.3 ± 1.8 c	7.2 ± 0.2 d	11.7 ± 0.3 d	414.2 ± 23.6 e	2.19 ± 0.11 c	1.64 ± 0.18 a	322.5 ± 18.8 a	179.7 ± 5.2 a	3.94 ± 0.29 a
Terrestrial average	**80.5 ± 1.1 A**	**9.7 ± 1.1 D**	**15.3 ± 1.7 C**	**439.0 ± 16.4 B**	**2.72 ± 0.26 BC**	**1.62 ± 0.09 A**	**304.6 ± 13.6 A**	**180.1 ± 4.1 A**	**3.69 ± 0.18 A**
Ceratophyllum demersum	82.7 ± 1.2 bc	14.9 ± 1.4 cd	23.1 ± 2.0 bcd	525.5 ± 48.3 de	3.61 ± 0.19 a	1.48 ± 0.04 a	239.9 ± 25.6 ab	158.3 ± 10.8 a	1.84 ± 0.20 c
Vallisneria gigantea	82.0 ± 0.6 bc	13.2 ± 1.1 cd	25.3 ± 3.5 bcd	401.9 ± 112.2 e	3.44 ± 0.17 a	1.18 ± 0.33 a	263.8 ± 21.4 ab	152.8 ± 19.3 a	1.81 ± 0.13 c
Freshwater average	**82.4 ± 0.6 A**	**13.9 ± 0.9 C**	**24.5 ± 2.2 B**	**451.3 ± 70.1 B**	**3.51 ± 0.13 A**	**1.30 ± 0.20 A**	**251.8 ± 16.1 A**	**155.6 ± 10.3 B**	**1.83 ± 0.11 B**
Stuckenia pectinata	81.6 ± 0.8 bc	25.0 ± 0.5 b	34.1 ± 1.5 ab	748.3 ± 145.1 cde	3.17 ± 0.24 ab	1.28 ± 0.19 a	128.8 ± 10.4 cd	88.3 ± 6.7 bc	0.94 ± 0.13 e
Ruppia cirrhosa	84.0 ± 0.7 b	17.8 ± 0.3 c	24.9 ± 0.8 bcd	642.1 ± 77.3 cde	3.27 ± 0.41 ab	1.18 ± 0.14 a	157.1 ± 22.4 bc	110.2 ± 13.3 b	1.35 ± 0.18 d
Brackish water average	**82.8 ± 0.7 A**	**21.4 ± 1.2 B**	**29.5 ± 1.7 B**	**699.3 ± 84.0 B**	**3.22 ± 0.22 AB**	**1.23 ± 0.11 A**	**141.4 ± 11.8 B**	**98.0 ± 7.5 C**	**1.17 ± 0.13 C**
Posidonia oceanica	91.0 ± 1.3 a	35.1 ± 1.4 a	43.6 ± 0.8 a	1.328.2 ± 179.5 a	2.17 ± 0.08 c	0.92 ± 0.15 a	65.2 ± 4.7 f	51.9 ± 4.5 d	0.49 ± 0.05 e
Cymodocea nodosa	90.4 ± 1.0 a	25.7 ± 0.9 b	32.5 ± 0.8 abc	983.9 ± 167.7 abc	2.75 ± 0.12 abc	1.13 ± 0.20 a	103.4 ± 1.6 de	80.6 ± 4.5 bcd	0.72 ± 0.01 e
Zostera marina	85.8 ± 2.3 b	25.3 ± 2.1 b	32.1 ± 3.1 ab	1,210.0 ± 167.6 ab	2.80 ± 0.10 abc	1.42 ± 0.13 a	108.8 ± 8.7 de	81.2 ± 4.5 bcd	0.79 ± 0.05 e
Zostera noltii	72.8 ± 1.2 d	29.8 ± 0.9 ab	39.7 ± 3.6 a	851.9 ± 68.5 bcd	2.57 ± 0.17 bc	1.01 ± 0.17 a	87.6 ± 6.0 ef	61.4 ± 7.1 cd	0.76 ± 0.06 e
Seawater average	**85.1 ± 1.9 A**	**29.0 ± 1.1 A**	**37.0 ± 1.7 A**	**1,066.7 ± 78.0 A**	**2.51 ± 0.08 C**	**1.12 ± 0.09 A**	**89.5 ± 4.7 C**	**67.9 ± 4.1 D**	**0.69 ± 0.04 D**
P^1	1.43×10^{-8}	2.77×10^{-6}	0.0003	0.0012	0.0001	0.0635	1.38×10^{-5}	1.33×10^{-10}	9.17×10^{-17}
P^2	0.1904	1.14×10^{-14}	4.19×10^{-8}	2.26×10^{-5}	8.80×10^{-5}	0.1157	1.13×10^{-7}	1.34×10^{-13}	5.48×10^{-7}

720 **Table 2. Photosynthesis-CO_2 curves.** Photosynthetic semi-saturation constant for CO_2 and DIC *in vivo* ($K_{m\ in\ vivo}$ CO_2 and $K_{m\ in\ vivo}$ DIC,
721 respectively; n = 5-8), and maximum net photosynthetic rate *in vivo* ($A_{n\ max}$, n = 5-8) obtained from photosynthesis-CO_2 curves. A_n was measured
722 in terrestrial species by means of gas exchange measurements using an open infrared gas-exchange analyzer system, whereas A_n was measured in
723 aquatic species by means of O_2 evolution in their respective aquatic medium. Different small letters show significant differences among species
724 (P^1) and capital letters show significant differences among environments (P^2). P^1 and P^2 values were obtained from the F-statistic of one-way
725 ANOVA or from the chi-squared value of Kruskal–Wallis test in the case of non-parametric data. Duncan's test and Kruskal–Wallis test followed
726 by Bonferroni correction for non-parametric data were used to detect differences among means.
727
728

Species / environment	$A_{n\ max}$ *in vivo* (μmol O_2 or CO_2 m^{-2} s^{-1})	K_m *in vivo* CO_2 (μM)	K_m *in vivo* DIC (mM)
Alisma lanceolatum	36.09 ± 2.43 a	26.3 ± 0.9 bc	-
Triglochin maritima	45.69 ± 2.11 a	34.4 ± 1.3 ab	-
Terrestrial average	**40.89 ± 2.20 A**	**30.8 ± 1.6 B**	-
Ceratophyllum demersum	2.91 ± 0.35 bc	71.2 ± 3.5 a	2.89 ± 0.28 ab
Vallisneria Gigantea	2.33 ± 0.18 cd	81.8 ± 4.5 a	3.60 ± 0.20 a
Freshwater average	**2.68 ± 0.23 C**	**75.5 ± 3.0 A**	**3.17 ± 0.20 A**
Stuckenia pectinata	4.91 ± 0.54 ab	29.6 ± 2.1 b	1.07 ± 0.07 cd
Ruppia cirrhosa	5.47 ± 0.71 ab	13.7 ± 1.0 cd	1.34 ± 0.10 bc
Brackish water average	**5.21 ± 0.45 B**	**21.2 ± 2.4 B**	**1.21 ± 0.07 B**
Posidonia oceanica	1.83 ± 0.10 d	5.2 ± 0.3 f	0.73 ± 0.04 e
Cymodocea nodosa	1.61 ± 0.25 d	6.2 ± 0.3 ef	0.87 ± 0.04 de
Zostera marina	2.36 ± 0.12 cd	13.3 ± 2.3 de	1.47 ± 0.25 cd
Zostera noltii	1.54 ± 0.35 d	4.9 ± 0.3 f	0.71 ± 0.04 e
Seawater average	**1.83 ± 0.12 D**	**7.1 ± 0.7 C**	**0.91 ± 0.07 C**
P^1	4.48×10^{-9}	4.73×10^{-11}	1.72×10^{-8}
P^2	1.16×10^{-11}	5.01×10^{-13}	1.49×10^{-9}

729

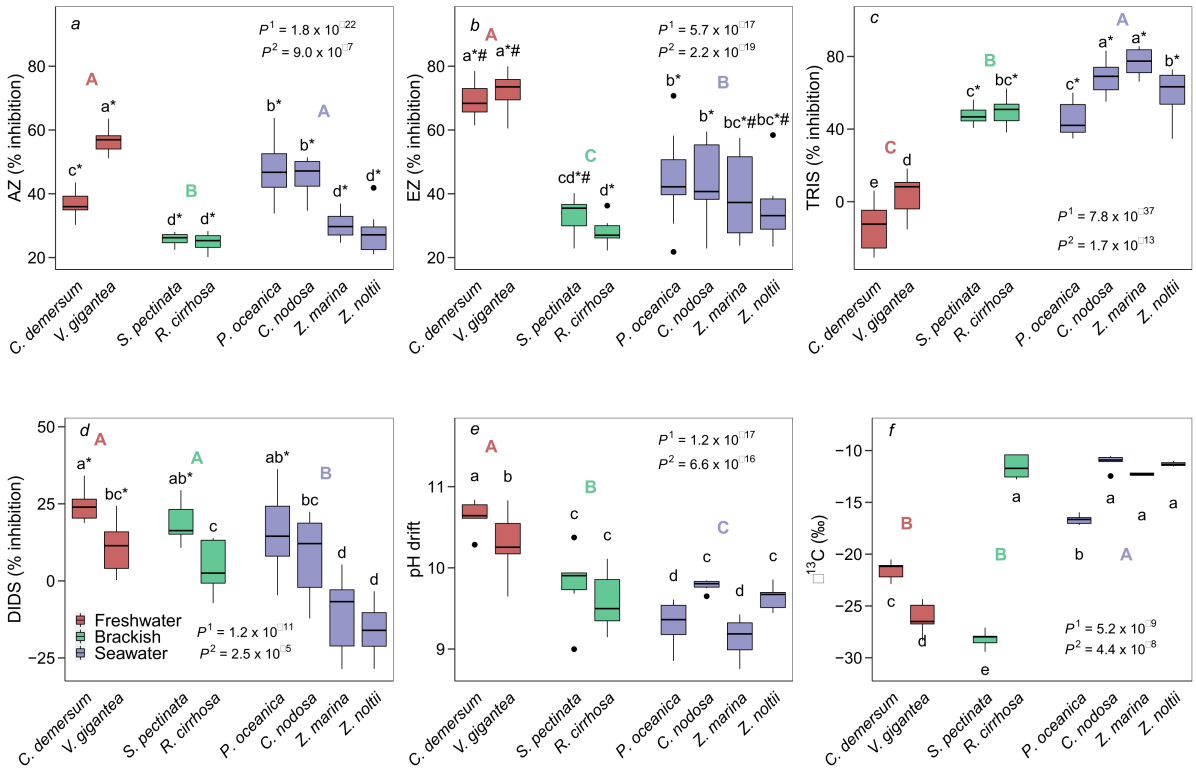

730

731 **Fig. 1. Boxplots of the indirect proxies for the CO_2 concentrating mechanisms of**
732 **aquatic angiosperms.** Parameters plotted are the percentage of net photosynthetic rate
733 inhibition after addition of acetazolamide (AZ, ***a***, n = 9), ethoxyzolamide (EZ, ***b***, n = 9),
734 TRIS-buffer (TRIS, ***c***, n = 10) and 4,4'-diisothiocyanatostilbene-2,2'-disulfonate (DIDS,
735 ***d***, n = 8); pH compensation points determined by pH-drift assays (pH drift, ***e***, n = 9, pH
736 compensation points below 9 in seawater, 9.3 in brackish water and 9.5 in freshwater
737 means only diffusive CO_2 entry), and isotopic composition of ^{13}C from leaf biomass
738 ($\delta^{13}C$, ***f***, n = 6). Black lines inside boxes indicate the data median, bound of boxes delimits
739 the 25th–75th percentile of the date and whiskers represent the 1.5 interquartile range
740 limits. * Indicates statistically significant inhibition on the net photosynthetic rate ($P < 0.05$) and # indicates significant differences between the net photosynthetic rate under the
741 presence of AZ and EZ ($P < 0.05$). In both cases, P values were determined using two-
742 sided Student's t-test or two-sided Mann-Whitney-Wilcoxon for non-parametric data.
743 Different small letters show significant differences among species (P^1) and capital letters
744

745 show significant differences among environments (P^2). P^1 and P^2 values were obtained
746 from the F-statistic of one-way ANOVA or from the chi-squared value of Kruskal–Wallis
747 test in the case of non-parametric data. Duncan's test and Kruskal–Wallis test followed
748 by Bonferroni correction for non-parametric data were used to detect differences among
749 means.
750
751
752
753
754
755
756
757
758
759
760
761
762

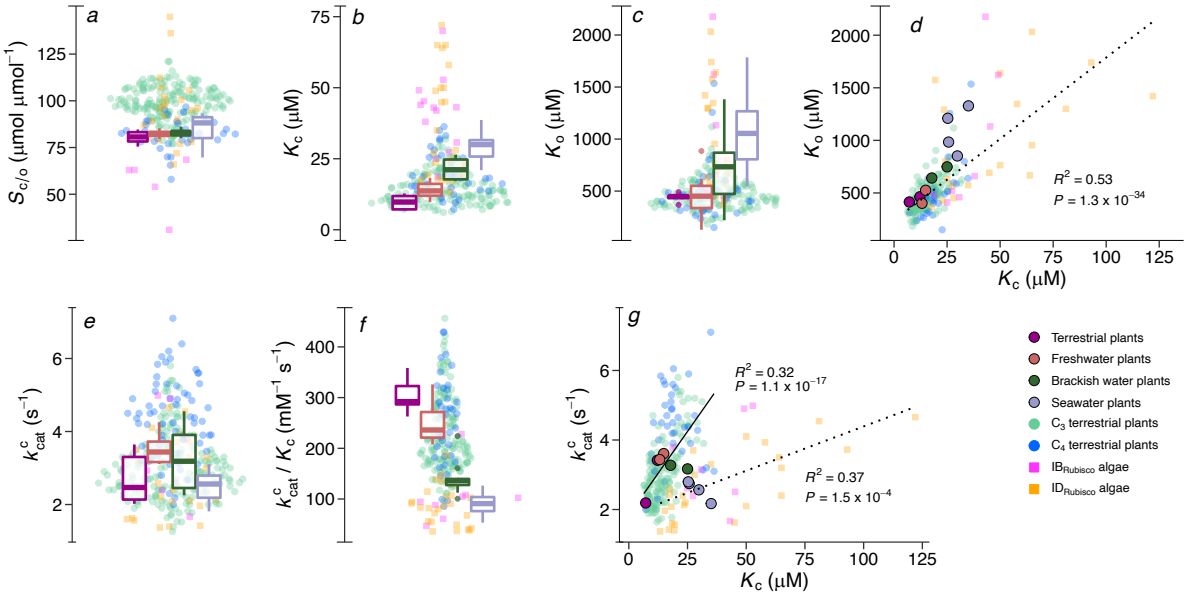

763

764 **Fig. 2. Boxplots of the Rubisco kinetic parameters from the analyzed species**
765 **compared with the Rubisco kinetic parameters from terrestrial plants (C_3 and C_4**
766 **species) and eukaryotic algae (form IB or ID Rubisco) possessing CO_2 concentrating**
767 **mechanisms compiled by Iñiguez *et al.*[21] and Goudet *et al.*[23].** Parameters shown are the
768 Rubisco CO_2/O_2 specificity (***a***, $S_{c/o}$, n = 237), the Michaelis–Menten constant for CO_2 (***b***,
769 K_c, n = 247) and for O_2 (***c***, K_o, n = 205), the maximum carboxylation rate (***e***, k_{cat}^c, n =
770 286) and the carboxylation catalytic efficiency (***f***, k_{cat}^c/K_c, n = 225). Panel ***d*** shows the
771 relationship between K_c and K_o among all species compiled (n = 205); panel ***g*** shows the
772 relationship between k_{cat}^c and K_c for terrestrial C_3 and C_4 plants (solid line, n = 191) and
773 for algal species (dotted line, n = 34); big points are the measured values for the species
774 analyzed in the present study. Black lines inside boxes indicate the data median, bound
775 of boxes delimits the 25th–75th percentile of the date and whiskers represent the 1.5
776 interquartile range limits. The width of the jitter in a-c, and e- f is controlled by the density
777 distribution of the data within each class. P values in ***d*** and ***g*** were obtained from two-
778 sided test for association between paired samples based in Pearson's correlation
779 coefficient.

780

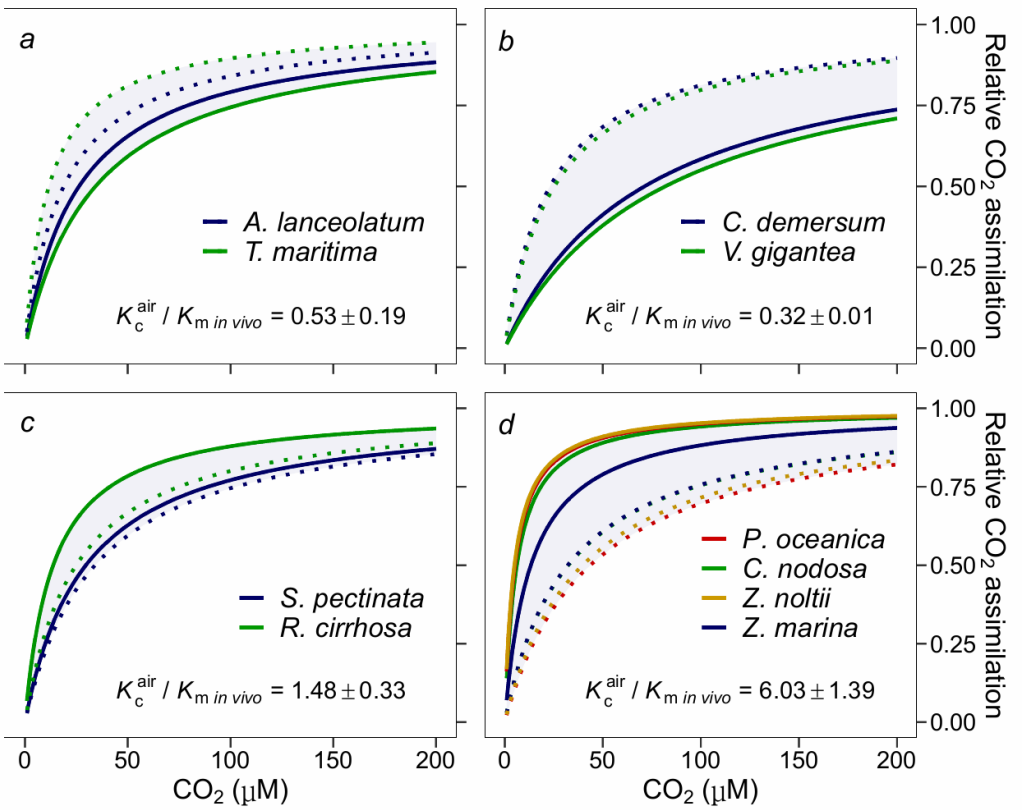

781

782 **Fig. 3. CO_2 concentrating mechanism effectiveness to deliver CO_2 to Rubisco**.
783 Measured photosynthesis *in vivo* (solid line) and *in vitro* Rubisco carboxylation under
784 ambient O_2 (dotted line) response to different CO_2 concentrations for ***a*,** terrestrial species;
785 ***b*,** freshwater species; ***c*,** brackish water species and ***d***, marine species. Maximum Rubisco
786 and photosynthetic CO_2 assimilation rate was standardized to 1 in all plots. The *in vitro*
787 Rubisco carboxylation and *in vivo* photosynthetic CO_2 assimilation response to different
788 CO_2 concentrations were both measured under ambient O_2. The species mean and s.e. for
789 the ratio between the *in vitro* Rubisco semi-saturation constant for CO_2 under ambient O_2
790 (K_c^{air}) and the *in vivo* photosynthetic semi-saturation constant for CO_2 ($K_{m\ in\ vivo}$) are
791 shown for the freshwater, brackish water, seawater and terrestrial angiosperms in each
792 plot.

793

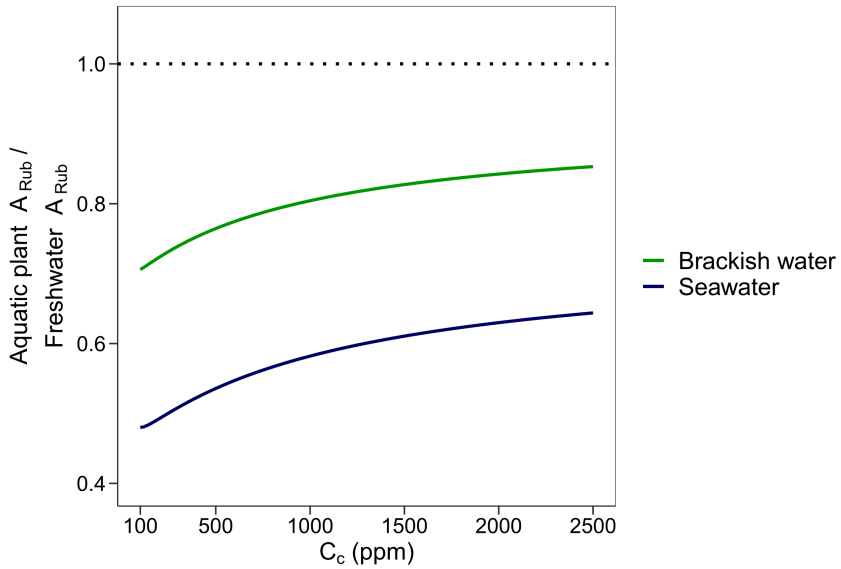

794

795 **Fig. 4. Ratio of the modelled Rubisco gross assimilation rate (A_{Rub}) between either**
796 **brackish water or marine Rubisco and freshwater Rubisco**. The photosynthesis model
797 of Farquhar et al.[41] was used to model A_{Rub} at a range of chloroplastic CO_2 concentrations
798 (C_c). This modelling exercise assumes CO_2 assimilation rates under saturating light
799 conditions.

800

801

802

803

804

805

806

807

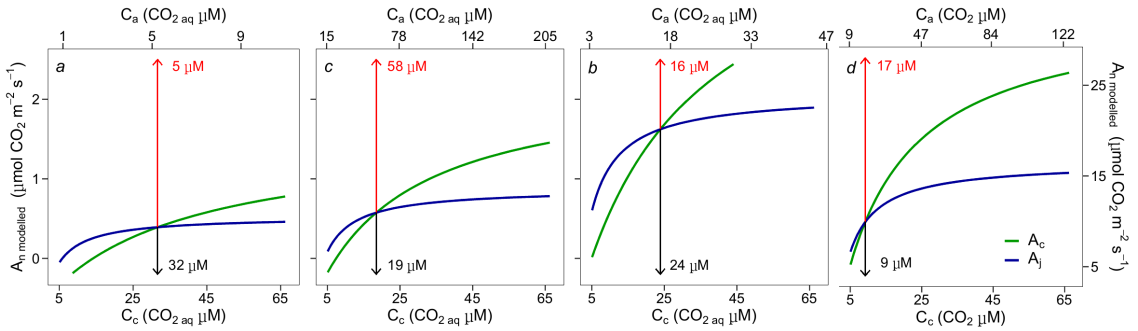

Fig. 5. Modelled leaf net photosynthetic rate as a function of chloroplastic CO_2 (C_c) using equations of the photosynthetic C_3 model of Farquhar et al.[41] and average Rubisco kinetic data of the species from each environment. ***a***, seawater species; ***b***, brackish water species; ***c***, freshwater species; ***d*** terrestrial species. Blue respresents the Rubisco-limited rate of CO_2 assimilation (A_c), and green, the electron-transport limited rate of CO_2 assimilation (A_j). The equivalent extracellular CO_2 concentration (C_a) is shown in the upper *x* axis.

References

1. Duarte, B. *et al.* Climate change impacts on seagrass meadows and macroalgal forests: An integrative perspective on acclimation and adaptation potential. *Front. Mar. Sci.* **5**, (2018).
2. Costanza, R. *et al.* Changes in the global value of ecosystem services. *Glob. Environ. Chang.* **26**, 152–158 (2014).
3. Zeebe, R. E. On the molecular diffusion coefficients of dissolved CO2, HCO3-, and CO32- and their dependence on isotopic mass. *Geochim. Cosmochim. Acta* **75**, 2483–2498 (2011).
4. Mass, T., Genin, A., Shavit, U., Grinstein, M. & Tchernov, D. Flow enhances photosynthesis in marine benthic autotrophs by increasing the efflux of oxygen

828 from the organism to the water. *Proc. Natl. Acad. Sci. U. S. A.* **107**, 2527–2531
829 (2010).
830 5. Skirrow, G. The dissolved gases-carbon dioxide. in *Chemical Oceanography, Vol.*
831 *2* (eds. Riley, J. P. & Skirrow, G.) 192 (Academic Press, 1975).
832 6. Stumm, W. & Morgan, J. J. *Aquatic chemistry: chemical equilibria in natural*
833 *waters*. (John Wiley & Sons, 2012).
834 7. Maberly, S. C. & Gontero, B. Ecological imperatives for aquatic CO2-
835 concentrating mechanisms. *J. Exp. Bot.* **68**, 3797–3814 (2017).
836 8. Maberly, S. C. Diel, episodic and seasonal changes in pH and concentrations of
837 inorganic carbon in a productive lake. *Freshw. Biol.* **35**, 579–598 (1996).
838 9. Meybeck, M. Global Occurrence of Major Elements in Rivers. in *Treatise on*
839 *Geochemistry* (eds. Holland, Heinrich, D. & Turekian, K. K.) vol. 5 207–223
840 (Elsevier Science Publishing, 2003).
841 10. Giordano, M., Beardall, J. & Raven, J. A. CO2 concentrating mechanisms in algae:
842 mechanisms, environmental modulation, and evolution. *Annu. Rev. Plant Biol.* **56**,
843 99–131 (2005).
844 11. Beer, S., Shomer-Ilan, A. & Waisel, Y. Carbon Metabolism in Seagrasses. *J. Exp.*
845 *Bot.* **31**, 1027–1033 (1980).
846 12. Raven, J. A., Cockell, C. S. & De La Rocha, C. L. The evolution of inorganic
847 carbon concentrating mechanisms in photosynthesis. *Philos. Trans. R. Soc. B Biol.*
848 *Sci.* **363**, 2641–2650 (2008).
849 13. Yin, L., Li, W., Madsen, T. V., Maberly, S. C. & Bowes, G. Photosynthetic
850 inorganic carbon acquisition in 30 freshwater macrophytes. *Aquat. Bot.* **140**, 48–
851 54 (2017).
852 14. Larkum, A. W. D., Davey, P. A., Kuo, J., Ralph, P. J. & Raven, J. A. Carbon-

concentrating mechanisms in seagrasses. *J. Exp. Bot.* **68**, 3773–3784 (2017).

15. Raven, J. A., Beardall, J. & Sánchez-Baracaldo, P. The possible evolution and future of CO2-concentrating mechanisms. *J. Exp. Bot.* **68**, 3701–3716 (2017).

16. Meyer, M. & Griffiths, H. Origins and diversity of eukaryotic CO2-concentrating mechanisms: lessons for the future. *J. Exp. Bot.* **64**, 769–786 (2013).

17. Badger, M. R. *et al.* The diversity and coevolution of Rubisco, plastids, pyrenoids, and chloroplast-based CO2-concentrating mechanisms in algae. *Can. J. Bot.* **76**, 1052–1071 (1998).

18. Savir, Y., Noor, E., Milo, R. & Tlusty, T. Cross-species analysis traces adaptation of Rubisco toward optimality in a low-dimensional landscape. *Proc. Natl. Acad. Sci. U. S. A.* **107**, 3475–3480 (2010).

19. Tcherkez, G. G. B., Farquhar, G. D. & Andrews, T. J. Despite slow catalysis and confused substrate specificity, all ribulose bisphosphate carboxylases may be nearly perfectly optimized. *Proc. Natl. Acad. Sci. U. S. A.* **103**, 7246–7251 (2006).

20. Flamholz, A. I. *et al.* Revisiting Trade-offs between Rubisco Kinetic Parameters. *Biochemistry* **58**, 3365–3376 (2019).

21. Iñiguez, C. *et al.* Evolutionary trends in RuBisCO kinetics and their co-evolution with CO2 concentrating mechanisms. *Plant J.* **101**, 897–918 (2020).

22. Genkov, T. & Spreitzer, R. J. Highly conserved small subunit residues influence Rubisco large subunit catalysis. *J. Biol. Chem.* **284**, 30105–30112 (2009).

23. Goudet, M. M. M. *et al.* Rubisco and carbon-concentrating mechanism co-evolution across chlorophyte and streptophyte green algae. *New Phytol.* **227**, 810–823 (2020).

24. Heureux, A. M. C. *et al.* The role of Rubisco kinetics and pyrenoid morphology in shaping the CCM of haptophyte microalgae. *J. Exp. Bot.* **68**, 3959–3969 (2017).

878 25. Young, J. N. *et al.* Large variation in the Rubisco kinetics of diatoms reveals
879 diversity among their carbon-concentrating mechanisms. *J. Exp. Bot.* **67**, 3445–
880 3456 (2016).
881 26. Lucas, W. J. Photosynthetic Assimilation of Exogenous HCO3- by Aquatic Plants.
882 *Annu. Rev. Plant Physiol.* **34**, 71–104 (1983).
883 27. Walker, N. A., Smith, F. A. & Cathers, I. R. Bicarbonate assimilation by fresh-
884 water charophytes and higher plants: I. Membrane transport of bicarbonate ions is
885 not proven. *J. Membr. Biol.* **57**, 51–58 (1980).
886 28. Rubio, L. *et al.* Direct uptake of HCO3− in the marine angiosperm Posidonia
887 oceanica (L.) delile driven by a plasma membrane H+ economy. *Plant Cell*
888 *Environ.* **40**, 2820–2830 (2017).
889 29. Iñiguez, C., Galmés, J. & Gordillo, F. J. L. Rubisco carboxylation kinetics and
890 inorganic carbon utilization in polar versus cold-temperate seaweeds. *J. Exp. Bot.*
891 **70**, 1283–1297 (2019).
892 30. Capó-Bauçà, S., Font-Carrascosa, M., Ribas-Carbó, M., Pavlovič, A. & Galmés, J.
893 Biochemical and mesophyll diffusional limits to photosynthesis are determined by
894 prey and root nutrient uptake in the carnivorous pitcher plant Nepenthes × ventrata.
895 *Ann. Bot.* **126**, 25–37 (2020).
896 31. Evans, J. R. Photosynthesis and nitrogen relationships in leaves of C3 plants.
897 *Oecologia* **78**, 9–19 (1989).
898 32. Raven, J. A. & Beardall, J. The ins and outs of CO2. *J. Exp. Bot.* **67**, 1–13 (2016).
899 33. Mohr, W. *et al.* Terrestrial-type nitrogen-fixing symbiosis between seagrass and a
900 marine bacterium. *Nature* **600**, 105–109 (2021).
901 34. Larkum, A. W. D., Orth, R. J. & Duarte, C. M. *Seagrass: Biology, Ecology and*
902 *Conservation. Springer Netherlands* (Springer Netherlands, 2006).

903 doi:https://doi.org/10.1007/978-1-4020-2983-7.
904 35. Les, D. H., Cleland, M. A. & Waycott, M. Phylogenetic studies in Alismatidae, II:
905 evolution of marine angiosperms (seagrasses) and hydrophily. *Syst. Bot.* **22**, 443–
906 463 (1997).
907 36. Ishikawa, C., Hatanaka, T., Misoo, S., Miyake, C. & Fukayama, H. Functional
908 incorporation of sorghum small subunit increases the catalytic turnover rate of
909 rubisco in transgenic rice. *Plant Physiol.* **156**, 1603–1611 (2011).
910 37. Lin, M. T., Stone, W. D., Chaudhari, V. & Hanson, M. R. Small subunits can
911 determine enzyme kinetics of tobacco Rubisco expressed in Escherichia coli. *Nat.*
912 *Plants* **6**, 1289–1299 (2020).
913 38. Raven, J. A., Ball, L. A., Beardall, J., Giordano, M. & Maberly, S. C. Algae lacking
914 carbon-concentrating mechanisms. *Can. J. Bot.* **83**, 879–890 (2005).
915 39. Young, J. N. & Hopkinson, B. M. The potential for co-evolution of CO2-
916 concentrating mechanisms and Rubisco in diatoms. *J. Exp. Bot.* **68**, 3751–3762
917 (2017).
918 40. Griffiths, H., Meyer, M. T. & Rickaby, R. E. M. Overcoming adversity through
919 diversity: Aquatic carbon concentrating mechanisms. *J. Exp. Bot.* **68**, 3689–3695
920 (2017).
921 41. Farquhar, G., Caemmerer, S. Von & Berry, J. A. A biochemical model of
922 photosynthetic CO2 assimilation in leaves of C3 species. *Planta* **90**, 78–90 (1980).
923 42. Wang, H. & Dilcher, D. L. A new species of Donlesia (Ceratophyllaceae) from the
924 Early Cretaceous of Kansas, USA. *Rev. Palaeobot. Palynol.* **252**, 20–28 (2018).
925 43. Galmés, J. *et al.* Environmentally driven evolution of Rubisco and improved
926 photosynthesis and growth within the C3 genus Limonium (Plumbaginaceae). *New*
927 *Phytol.* **203**, 989–999 (2014).

928 44. Sharwood, R. E., Ghannoum, O., Kapralov, M. V., Gunn, L. H. & Whitney, S. M.
929 Temperature responses of Rubisco from Paniceae grasses provide opportunities for
930 improving C 3 photosynthesis. *Nat. Plants* **2**, 1–9 (2016).
931 45. Wissler, L. *et al.* Back to the sea twice: identifying candidate plant genes for
932 molecular evolution to marine life. *BMC Evol. Biol.* **11**, 1–12 (2011).
933 46. Larkum, A. W. D., Kendrick, G. A. & Editors, P. J. R. *Seagrasses of Australia*.
934 *Seagrasses of Australia* (2018).
935 47. Berner, R. A. & Kothavala, Z. Geocarb III: A revised model of atmospheric CO2
936 over phanerozoic time. *Am. J. Sci.* **301**, 182–204 (2001).
937 48. Sage, R. F., Monson, R. K., Ehleringer, J. R., Adachi, S. & Pearcy, R. W. Some
938 like it hot: the physiological ecology of C4 plant evolution. *Oecologia* **187**, 941–
939 966 (2018).
940 49. Chen, L. Y., Chen, J. M., Gituru, R. W. & Wang, Q. F. Generic phylogeny,
941 historical biogeography and character evolution of the cosmopolitan aquatic plant
942 family Hydrocharitaceae. *BMC Evol. Biol.* **12**, 30 (2012).
943 50. Janssen, T. & Bremer, K. The age of major monocot groups inferred from 800+
944 rbcL sequences. *Bot. J. Linn. Soc.* **146**, 385–398 (2004).
945 51. Lindqvist, C. *et al.* Molecular phylogenetics of an aquatic plant lineage,
946 Potamogetonaceae. *Cladistics* **22**, 568–588 (2006).
947 52. Yao, G. *et al.* Phylogenetic relationships, character evolution and biogeographic
948 diversification of Pogostemon s.l. (Lamiaceae). *Mol. Phylogenet. Evol.* **98**, 184–
949 200 (2016).
950 53. Gomez, B. *et al.* Montsechia vidalii from the Barremian of Spain, the earliest
951 known submerged aquatic angiosperm, and its systematic relationship to
952 Ceratophyllum. *Taxon* **69**, 1273–1292 (2020).

953 54. Bouvier, J. W. *et al.* Rubisco Adaptation Is More Limited by Phylogenetic
954 Constraint Than by Catalytic Trade-off. *Mol. Biol. Evol.* **38**, 2880–2896 (2021).
955 55. Kim, M. *et al.* Low oxygen affects photophysiology and the level of expression of
956 two-carbon metabolism genes in the seagrass Zostera muelleri. *Photosynth. Res.*
957 **136**, 147–160 (2018).
958 56. Roberts, D. G. & Moriarty, D. J. W. Lacunal gas discharge as a measure of
959 productivity in the seagrasses Zostera capricorni, Cymodocea serrulata and
960 Syringodium isoetifolium. *Aquat. Bot.* **28**, 143–160 (1987).
961 57. Bowes, G., Rao, S. K., Estavillo, G. M. & Reiskind, J. B. C4 mechanisms in aquatic
962 angiosperms: Comparisons with terrestrial C4 systems. *Funct. Plant Biol.* **29**, 379–
963 392 (2002).
964 58. Invers, O., Zimmerman, R. C., Alberte, R. S., Pérez, M. & Romero, J. Inorganic
965 carbon sources for seagrass photosynthesis: An experimental evaluation of
966 bicarbonate use in species inhabiting temperate waters. *J. Exp. Mar. Bio. Ecol.* **265**,
967 203–217 (2001).
968 59. Lewis, E. & Wallace, D. *Program Developed for CO2 System Calculations*.
969 (Carbon Dioxide Information Analysis Center, Oak Ridge National Laboratory,
970 1998).
971 60. Price, G. . & Badger, M. . Inhibition by proton buffers of photosynthetic utilization
972 of bicarbonate in Chara corallina. *Aust. J. Plant Physiol.* **12**, 257–267 (1985).
973 61. Beer, S., Bjork, M., Hellblom, F. & Axelsson, L. Inorganic carbon utilization in
974 marine angiosperms (seagrasses). *Funct. Plant Biol.* **29**, 349–354 (2002).
975 62. Galmés, J., Medrano Hip, 'lito & Flexas, J. Photosynthetic limitations in response
976 to water stress and recovery in Mediterranean plants with different growth forms.
977 *New Phytol.* **175**, 81–93 (2007).

978 63. Flexas, J. *et al.* Analysis of leakage in IRGA's leaf chambers of open gas exchange
979 systems: Quantification and its effects in photosynthesis parameterization. *J. Exp.*
980 *Bot.* **58**, 1533–1543 (2007).
981 64. Iñiguez, C. *et al.* Increased temperature, rather than elevated CO2, modulates the
982 carbon assimilation of the Arctic kelps Saccharina latissima and Laminaria
983 solidungula. *Mar. Biol.* **163**, (2016).
984 65. Galmés, J. *et al.* Expanding knowledge of the Rubisco kinetics variability in plant
985 species: Environmental and evolutionary trends. *Plant, Cell Environ.* **37**, 1989–
986 2001 (2014).
987 66. Ruuska, S. *et al.* The interplay between limiting processes in C3 photosynthesis
988 studied by rapid-response gas exchange using transgenic tobacco impaired in
989 photosynthesis. *Aust. J. Plant Physiol.* **25**, 859–870 (1998).
990 67. Bradford, M. M. A rapid and sensitive method for the quantitation of microgram
991 quantities of protein utilizing the principle of protein-dye binding. *Anal. Biochem.*
992 **72**, 248–254 (1976).
993 68. Sharwood, R. E., Von Caemmerer, S., Maliga, P. & Whitney, S. M. The catalytic
994 properties of hybrid rubisco comprising tobacco small and sunflower large
995 subunits mirror the kinetically equivalent source rubiscos and can support tobacco
996 growth. *Plant Physiol.* **146**, 83–96 (2008).
997 69. Kane, H. *et al.* An Improved Method for Measuring the CO2 /O2 Specificity of
998 Ribulosebisphosphate Carboxylase-Oxygenase. *Aust. J. Plant Physiol.* **21**, 449
999 (1994).
1000 70. Galmés, J., Hermida-Carrera, C., Laanisto, L. & Niinemets, Ü. A compendium of
1001 temperature responses of Rubisco kinetic traits: variability among and within
1002 photosynthetic groups and impacts on photosynthesis modeling. *J. Exp. Bot.* **67**,

5067–5091 (2016).

71. Archontoulis, S. V., Yin, X., Vos, J., Danalatos, N. G. & Struik, P. C. Leaf photosynthesis and respiration of three bioenergy crops in relation to temperature and leaf nitrogen: How conserved are biochemical model parameters among crop species? *J. Exp. Bot.* **63**, 895–911 (2012).

72. Hedges, S. B., Marin, J., Suleski, M., Paymer, M. & Kumar, S. Tree of life reveals clock-like speciation and diversification. *Mol. Biol. Evol.* **32**, 835–845 (2015).

73. Kumar, S., Stecher, G., Suleski, M. & Hedges, S. B. TimeTree: A Resource for Timelines, Timetrees, and Divergence Times. *Mol. Biol. Evol.* **34**, 1812–1819 (2017).

74. Tamura, K. Estimation of the number of nucleotide substitutions when there are strong transition-transversion and G+C-content biases. *Mol. Biol. Evol.* **9**, 678–687 (1992).

75. Kumar, S., Stecher, G., Li, M., Knyaz, C. & Tamura, K. MEGA X: Molecular evolutionary genetics analysis across computing platforms. *Mol. Biol. Evol.* **35**, 1547–1549 (2018).

76. Yang, Z. PAML 4: Phylogenetic analysis by maximum likelihood. *Mol. Biol. Evol.* **24**, 1586–1591 (2007).

77. Zhang, J., Nielsen, R. & Yang, Z. Evaluation of an improved branch-site likelihood method for detecting positive selection at the molecular level. *Mol. Biol. Evol.* **22**, 2472–2479 (2005).

Supplementary information

a

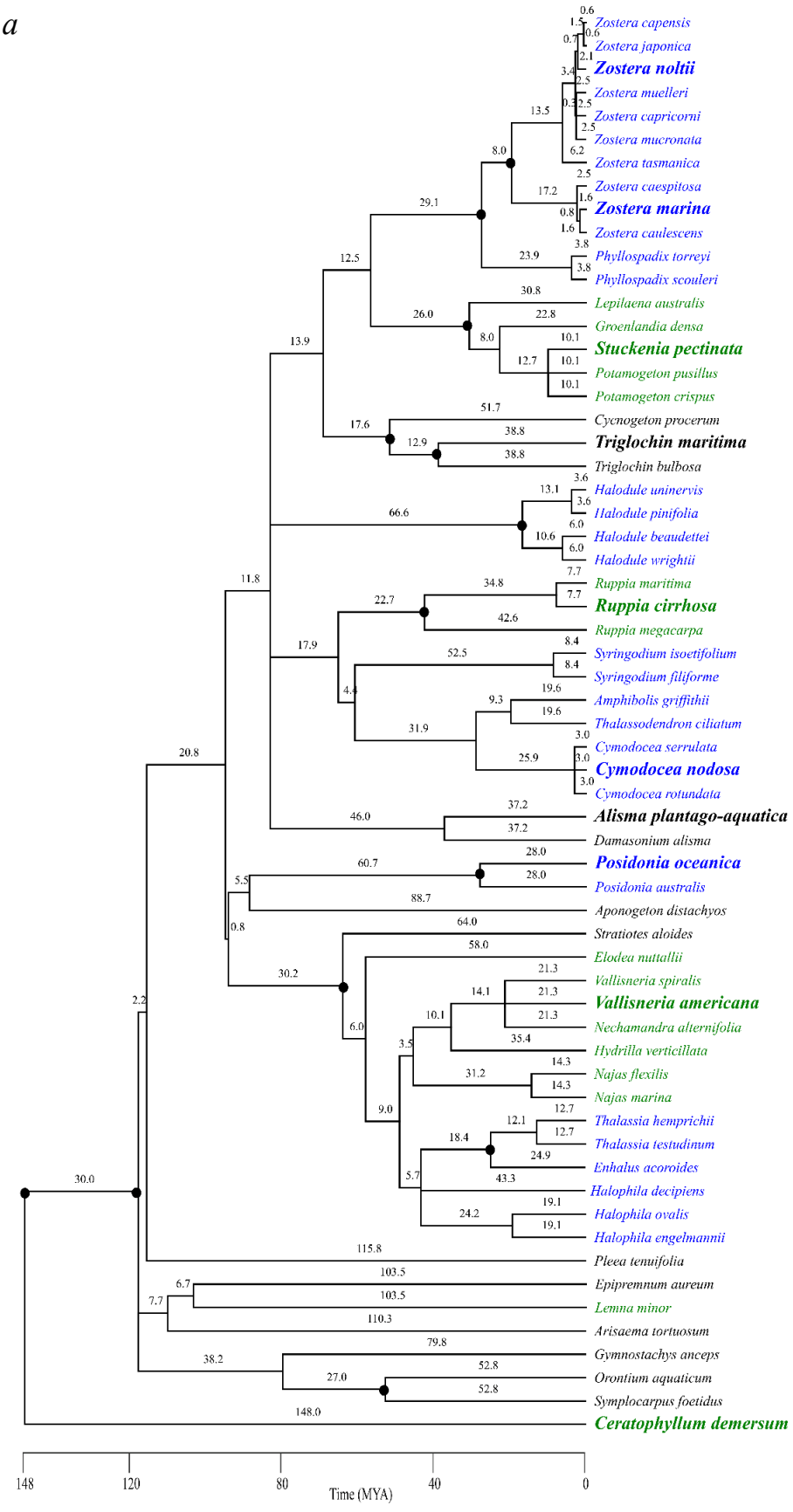

b

	Genes used in the analysis of Timetree
[1]	*accD, atpA, atpB, atpE, atpF, atpH, atpI, ccsA, cemA, clpP, infA, matK, ndhA, ndhB, ndhC, ndhD, ndhE, ndhF, ndhG, ndhH, ndhI, ndhJ, ndhK, petA, petB, petD, petG, petL, petN, psaA, psaB, psaC, psaI, psaJ, psbA, psbB, psbC, psbD, psbE, psbF, psbH, psbI, psbJ, psbK, psbL, psbM, psbN, psbT, rbcL, rpl2, rpl14, rpl16, rpl20, rpl22, rpl23, rpl32, rpl33, rpl36, rpoA, rpoB, rpoC1, rpoC2, rps2, rps3, rps4, rps7, rps8, rps11, rps12, rps14, rps15, rps16, rps18, rps19, rrn4.5, rrn5, rrn16, rrn23, ycf1, ycf2, ycf3, ycf4, PHYC* and *trnK/matK*
[2]	*rbcL, atpB, matR* and *18S*
[3]	*rbcL, 18S* and *atpB*
[4]	*rbcL*
[5]	*ITS, rbcL, matK* and *psbA*
[6]	*18S, rbcL, matK, trnK 5' intron, rpoB, rpoC1, cob* and *atp1*
[7]	*rbcL, matK* and *nadhF*
[8]	*atpB, psaA, psaB, psbA, psbB, rbcL* and *rps4*
[9]	*ITS1, matK, rbcL* and *psbA-trnH*
[10]	*matK* and *26S*
[11]	*rbcL, ITS* and *18S*
[12]	*rbcL* and *matK*
[13]	*rbcL, atpB, rps4, 18S* and *26S*
[14]	79 chloroplast protein-coding genes (Supplementary information not available)
[15]	*rbcL, matK, atpB* and *18S*
[16]	*rbcL*
[17]	*atpB, matK, ndhF, rbcL, atpA, 18S, 26S* and *PHYC*
[18]	*matK, ndhF, rbcL, rpoB, rpoC1* and *PHYC*
[19]	*rbcL*
[20]	*rbcL* and *matK*
[21]	*ITS, matK, rbcL, rpl16 and trnK*
[22]	*atpB, psaA, psbB* and *rbcL*
[23]	*atpB, psaA, psbB* and *rbcL*
[24]	*atpB, psaA, psbB* and *rbcL*
[25]	*atpB, matK, trnL intron, trnL-trnF spacer, ndhF, rbcL, atp1, matR, mtSSU, mtLSU, 18S* and *26S*
[26]	*18S, atpA, matR* and *nad1b-c intron*
[27]	*atpA, atpB, atpE, atpF, atpH, atpI, ccsA, cemA, clpP, matK, petA, petB, petD, petG, petL, petN, psaA, psaB, psaC, psaI, psaJ, psbA, psbB, psbC, psbD, psbE, psbF, psbH, psbI, psbJ, psbK, psbL, psbM, psbN, psbT, psbZ, rbcL, rpl14, rpl16, rpl2, rpl20, rpl32, rpl33, rpl36, rpoA, rpoB, rpoC1, rpoC2, rps11, rps12, rps14, rps15, rps18, rps19, rps2, rps3, rps4, rps7, rps8, ycf3* and *ycf4*
[28]	*trnL, matK, trnK* and *rbcL*
[29]	*18S, rbcL, atpB, atpA, matR, At3g47810, At2g32520, At3g52300, At5g06360, At5g04600, At2g21870, At4g33250, At4g30010, At4g08230, At4g31720, At4g37830, At5g47570, At5g23290* and *At2g13360*
[30]	*trnLF* and *ndhF*
[31]	*rbcL*

[32]	*rbcL, rps4, rbcL, atpB* and *18S*
[33]	*atpB, rbcL,* and *18S*
[34]	*rbcL, matK, ITS* and *psbA-trnH*
[35]	*rbcL, atpB* and *18S*
[36]	*accD, atpA, atpB, atpE, atpF, atpH, atpI, ccsA, cemA, clpP, HpsbI, infA, matK, ndhA, ndhB, ndhC, ndhD, ndhE, ndhF, ndhG, ndhH, ndhI, ndhJ, ndhK, petA, petB, petD, petG, petL, petN, psaA, psaB, psaC, psaI, psaJ, psb, psbA, psbB, psbC, psbD, psbE, psbF, psbJ, psbK, psbL, psbM, psbN, psbT, psbZ, rbcL, rpl14, rpl16, rpl2, rpl20, rpl22, rpl23, rpl32, rpl33, rpl36, rpoA, rpoB, rpoC1, rpoC2, rps11, rps12, rps14, rps15, rps16, rps18, rps19, rps2, rps3, rps4, rps7, rps8, ycf1, ycf2, ycf3* and *ycf4*
[37]	*accD, atpA, atpB, atpE, atpF, atpH, atpI, ccsA, cemA, clpP, infA, matK, ndhA, ndhB, ndhC, ndhD, ndhE, ndhF, ndhG, ndhH, ndhI, ndhJ, ndhK, petA, petB, petD, petG, petL, petN, psaA, psaB, psaC, psaI, psaJ, psbA, psbB, psbC, psbD, psbE, psbF, psbH, psbI, psbJ, psbK, psbL, psbM, psbN, psbT, psbZ, rbcL, rpl2, rpl14, rpl16, rpl20, rpl22, rpl23, rpl32, rpl33, rpl36, rpoA, rpoB, rpoC1, rpoC2, rps2, rps3, rps4, rps7, rps8, rps11, rps12, rps14, rps15, rps16, rps18, rps19, ycf1, ycf2, ycf3, ycf4, rrn4.5, rrn5, rrn16* and *rrn23*
[38]	*MC1, SMC2, MCM5, MSH1, MLH1, accD, atpA, atpB, atpE, atpF, atpH, atpI, ccsA, cemA, clpP, infA, matK, ndhA, ndhB, ndhC, ndhD, ndhE, ndhF, ndhG, ndhH, ndhI, ndhJ, ndhK, petA, petB, petD, petG, petL, petN, psaA, psaB, psaC, psaI, psaJ, psbA, psbB, psbC, psbD, psbE, psbF, psbH, psbI, psbJ, psbK, psbL, psbM, psbN, psbT, psbZ, rbcL, rpl14, rpl16, rpl2, rpl20, rpl22, rpl23, rpl32, rpl33, rpl36, rpoA, rpoB, rpoC1, rpoC2, rps11, rps12, rps14, rps15, rps16, rps18, rps19, rps2, rps3, rps4, rps7, rps8, rrn16, rrn23, rrn4.5, rrn5, Total, trnN, ycf1* and *ycf2*
[39]	*SMC1, SMC2,MSH1, MLH1* and *MCM5*
[40]	*atpA, atpB, atpE, atpF, atpH, atpI, ccsA, cemA, clpP, matK, ndhA, ndhB, ndhC, ndhD, ndhE, ndhF, ndhG, ndhH, ndhI, ndhJ, ndhK, petA, petB, petD, petG, petL, petN, psaA, psaB, psaC, psaI, psaJ, psbA, psbB, psbC, psbD, psbE, psbF, psbH, psbI, psbJ, psbK, psbL, psbM, psbN, psbT, psbZ, rbcL, rpl14, rpl16, rpl2, rpl20, rpl22, rpl23, rpl32, rpl33, rpl36, rpoA, rpoB, rpoC1, rpoC2, rps11, rps12, rps14, rps15, rps16, rps18, rps19, rps2, rps3, rps4, rps7, rps8, rrn16, rrn23, rrn4.5, rrn5, ycf3, ycf3* and *ycf4*
[41]	*18S, rbcL, matK, trnK 5' intron, rpoB, rpoC1, cob and atp1*

References list:

1. Arakaki, M. *et al.* Contemporaneous and recent radiations of the world's major succulent plant lineages. *Proc. Natl. Acad. Sci. U. S. A.* **108**, 8379–8384 (2011).

2. Bell, C. D., Soltis, D. E. & Soltis, P. S. The age of the angiosperms: A molecular timescale without a clock. *Evolution (N. Y).* **59**, 1245–1258 (2005).

3. Bell, C. D., Soltis, D. E. & Soltis, P. S. The age and diversification of the angiosperms re-revisited. *Am. J. Bot.* **97**, 1296–1303 (2010).

4. Bremer, K. Early Cretaceous lineages of monocot flowering plants. *Proc. Natl. Acad. Sci. U. S. A.* **97**, 4707–4711 (2000).

5. Chen, L. Y., Chen, J. M., Gituru, R. W., Temam, T. D. & Wang, Q. F. Generic phylogeny and historical biogeography of Alismataceae, inferred from multiple DNA sequences.

Mol. Phylogenet. Evol. **63**, 407–416 (2012).

6. Chen, L. Y., Chen, J. M., Gituru, R. W. & Wang, Q. F. Generic phylogeny, historical biogeography and character evolution of the cosmopolitan aquatic plant family Hydrocharitaceae. *BMC Evol. Biol.* **12**, 30 (2012).

7. Christin, P. A. *et al.* Molecular dating, evolutionary rates, and the age of the grasses. *Syst. Biol.* **63**, 153–165 (2014).

8. Clarke, J. T., Warnock, R. C. M. & Donoghue, P. C. J. Establishing a time-scale for plant evolution. *New Phytol.* **192**, 266–301 (2011).

9. Coyer, J. A. *et al.* Phylogeny and temporal divergence of the seagrass family Zosteraceae using one nuclear and three chloroplast loci. *Syst. Biodivers.* **11**, 271–284 (2013).

10. Crisp, M. D. & Cook, L. G. Cenozoic extinctions account for the low diversity of extant gymnosperms compared with angiosperms. *New Phytol.* **192**, 997–1009 (2011).

11. Daru, B. H. & le Roux, P. C. Marine protected areas are insufficient to conserve global marine plant diversity. *Glob. Ecol. Biogeogr.* **25**, 324–334 (2016).

12. Dexter, K. & Chave, J. Evolutionary patterns of range size, abundance and species richness in Amazonian angiosperm trees. *PeerJ* **2016**, 1–14 (2016).

13. Fiz-Palacios, O., Schneider, H., Heinrichs, J. & Savolainen, V. Diversification of land plants: Insights from a family-level phylogenetic analysis. *BMC Evol. Biol.* **11**, (2011).

14. Foster, C. S. P. *et al.* Evaluating the impact of genomic data and priors on Bayesian estimates of the angiosperm evolutionary timescale. *Syst. Biol.* **66**, 338–351 (2017).

15. Harris, L. W. & Davies, T. J. A complete fossil-calibrated phylogeny of seed plant families as a tool for comparative analyses: Testing the 'time for speciation' hypothesis. *PLoS One* **11**, 1–16 (2016).

16. Hermant, M., Hennion, F., Bartish, I. V., Yguel, B. & Prinzing, A. Disparate relatives: Life histories vary more in genera occupying intermediate environments. *Perspect. Plant Ecol. Evol. Syst.* **14**, 283–301 (2012).

17. Hertweck, K. L. *et al.* Phylogenetics, divergence times and diversification from three genomic partitions in monocots. *Bot. J. Linn. Soc.* **178**, 375–393 (2015).

18. Ito, Y., Tanaka, N., García-Murillo, P. & Muasya, A. M. A new delimitation of the Afro-Eurasian plant genus Althenia to include its Australasian relative, Lepilaena (Potamogetonaceae) - Evidence from DNA and morphological data. *Mol. Phylogenet. Evol.* **98**, 261–270 (2016).

19. Janssen, T. & Bremer, K. The age of major monocot groups inferred from 800+ *rbcL* sequences. *Bot. J. Linn. Soc.* **146**, 385–398 (2004).

20. Kato, Y., Aioi, K., Omori, Y., Takahata, N. & Satta, Y. Phylogenetic analyses of *Zostera* species based on *rbcL* and *matK* nucleotide sequences: Implications for the origin and diversification of seagrasses in Japanese waters. *Genes Genet. Syst.* **78**, 329–342 (2003).

21. Les, D. H., Crawford, D. J., Kimball, R. T., Moody, M. L. & Landolt, E. Biogeography of discontinuously distributed hydrophytes: A molecular appraisal of intercontinental disjunctions. *Int. J. Plant Sci.* **164**, 917–932 (2003).

22. Magallón, S. A. & Sanderson, M. J. Angiosperm Divergence Times: the Effect of Genes, Codon Positions, and Time Constraints. *Evolution (N. Y).* **59**, 1653 (2005).

23. Magallón, S. Using fossils to break long branches in molecular dating: A comparison of

relaxed clocks applied to the origin of angiosperms. *Syst. Biol.* **59**, 384–399 (2010).

24. Magallón, S., Hilu, K. W. & Quandt, D. Land plant evolutionary timeline: Gene effects are secondary to fossil constraints in relaxed clock estimation of age and substitution rates. *Am. J. Bot.* **100**, 556–573 (2013).

25. Massoni, J., Couvreur, T. L. P. & Sauquet, H. Five major shifts of diversification through the long evolutionary history of Magnoliidae (angiosperms) Phylogenetics and phylogeography. *BMC Evol. Biol.* **15**, 1–14 (2015).

26. Mennes, C. B., Smets, E. F., Moses, S. N. & Merckx, V. S. F. T. New insights in the long-debated evolutionary history of Triuridaceae (Pandanales). *Mol. Phylogenet. Evol.* **69**, 994–1004 (2013).

27. Moore, M. J., Bell, C. D., Soltis, P. S. & Soltis, D. E. Using plastid genome-scale data to resolve enigmatic relationships among basal angiosperms. *Proc. Natl. Acad. Sci. U. S. A.* **104**, 19363–19368 (2007).

28. Nauheimer, L., Metzler, D. & Renner, S. S. Global history of the ancient monocot family Araceae inferred with models accounting for past continental positions and previous ranges based on fossils. *New Phytol.* **195**, 938–950 (2012).

29. Naumann, J. *et al.* Single-copy nuclear genes place haustorial Hydnoraceae within piperales and reveal a Cretaceous origin of multiple parasitic angiosperm lineages. *PLoS One* **8**, (2013).

30. Nie, Z. L., Sun, H., Li, H. & Wen, J. Intercontinental biogeography of subfamily Orontioideae (*Symplocarpus*, *Lysichiton*, and *Orontium*) of Araceae in eastern Asia and North America. *Mol. Phylogenet. Evol.* **40**, 155–165 (2006).

31. Sanderson, M. J. A nonparametric approach to estimating divergence times in the absence of rate constancy. *Mol. Biol. Evol.* **14**, 1218–1231 (1997).

32. Schneider, H. *et al.* Ferns diversified in the shadow of angiosperms. *Nature* **428**, 553–557 (2004).

33. Smith, S. A., Beaulieu, J. M. & Donoghue, M. J. An uncorrelated relaxed-clock analysis suggests an earlier origin for flowering plants. *Proc. Natl. Acad. Sci. U. S. A.* **107**, 5897–5902 (2010).

34. von Mering, S. & Kadereit, J. W. Phylogeny, biogeography and evolution of *Triglochin* L. (Juncaginaceae) - Morphological diversification is linked to habitat shifts rather than to genetic diversification. *Mol. Phylogenet. Evol.* **83**, 200–212 (2015).

35. Wikström, N., Savolainen, V. & Chase, M. W. Evolution of the angiosperms: Calibrating the family tree. *Proc. R. Soc. B Biol. Sci.* **268**, 2211–2220 (2001).

36. Wu, Z. *et al.* A precise chloroplast genome of *Nelumbo nucifera* (Nelumbonaceae) evaluated with Sanger, Illumina MiSeq, and PacBio RS II sequencing platforms: Insight into the plastid evolution of basal eudicots. *BMC Plant Biol.* **14**, 1–14 (2014).

37. Xue, J. H., Dong, W. P., Cheng, T. & Zhou, S. L. Nelumbonaceae: Systematic position and species diversification revealed by the complete chloroplast genome. *J. Syst. Evol.* **50**, 477–487 (2012).

38. Zeng, L. *et al.* Resolution of deep angiosperm phylogeny using conserved nuclear genes and estimates of early divergence times. *Nat. Commun.* **5**, (2014).

39. Zhang, N., Zeng, L., Shan, H. & Ma, H. Highly conserved low-copy nuclear genes as effective markers for phylogenetic analyses in angiosperms. *New Phytol.* **195**, 923–937 (2012).

40. Zhong, B., Yonezawa, T., Zhong, Y. & Hasegawa, M. Episodic evolution and adaptation of chloroplast genomes in ancestral grasses. *PLoS One* **4**, 1–9 (2009).

41. Zhu, J., Yu, D. & Xu, X. The phylogeographic structure of *Hydrilla verticillata* (Hydrocharitaceae) in China and its implications for the biogeographic history of this worldwide-distributed submerged macrophyte. *BMC Evol. Biol.* **15**, (2015).

Supplementary Fig. 1. Phylogenetic data obtained from Timetree website (http://www.timetree.org/) of the Alismatales species used in the analyses of positive selection. ***a***, phylogenetic tree obtained from the Timetree analysis. Details about the acquisition of Timetree data, their standardization, and the assembly of individual trees are available in Hedges et al.[1] and Kumar et al.[2]. In this method, the data from different phylogenetic studies are mapped on a guide tree from the National Center for Biotechnology Information (NCBI) Taxonomy Browser. Nodes marked with solid circles are those mapped directly to the NCBI Taxonomy, while the remaining nodes were created during the polytomy resolution process described in Hedges et al.[1]. Species coloured in blue are seagrasses, in green are hydrophiles/fully water submerged species (either freshwater or brackish water species) and in black are terrestrial species. The species selected in this study (or the most closely related species in the case of *Vallisneria gigantea* and *Alisma lanceolatum*) are indicated in bigger bold letters. Positive selection was detected in branches leading to fully water submerged plants (likelihood Ratio Test ($2\Delta\log_e L$) = 11.5, p-value = < 0.001). The positive selection was detected at positions 93 and 131 in the Rubisco large subunit of the branch leading to the species of the genera *Zostera*, *Phyllospadix*, *Lepilaena*, *Groenlandia*, *Stukenia* and *Potamogeton,* but this signal was not found in the other branches of aquatic plants, rejecting a generic role of these residues in the adaptation of Rubisco to the aquatic environment. No positive selection was detected in branches leading to seagrasses ($2\Delta\log_e L$ = 0.12, p-value >0.05). *Ceratophyllum demersum* was added as an outgroup and for comparative purposes; therefore, it was not included in the positive selection analyses. The final tree was obtained after an image edition of the files obtained from the Timetree website. The accession numbers of *rbc*L sequences used in the analyses of positive selection are: *Alisma plantago-aquatica* (L08759)*, Amphibolis griffithii* (HQ901574)*, Aponogeton distachyos* (U80684)*, Arisaema tortuosum* (AF497109)*, Ceratophyllum demersum* (D89473), *Cycnogeton procerum* (U80713), *Cymodocea nodosa* (KF488486), *Cymodocea rotundata* (KF488490), *Cymodocea serrulata* (KF488492), *Damasonium alisma* (U80678), *Elodea nuttallii* (U80696), *Enhalus acoroides* (U80697), *Epipremnum aureum* (AJ005625), *Groenlandia densa* (AB196954), *Gymnostachys anceps* (M91629), *Halodule beaudettei* (U80689), *Halodule pinifolia* (KF488494), *Halodule uninervis* (KF488495), *Halodule wrightii* (HQ901575), *Halophila decipiens* (U80698), *Halophila engelmannii* (U80699), *Halophila ovalis* (AB004890), *Hydrilla verticillata* (U80700), *Lemna minor* (AY034234), *Lepilaena australis* (U80729), *Najas flexilis* (U03731), *Najas marina* (U80705), *Nechamandra alternifolia* (U80706), *Orontium aquaticum* (AJ005632), *Phyllospadix scouleri* (DQ859172), *Phyllospadix torreyi* (U80731), *Pleea tenuifolia* (AJ131774), *Posidonia australis* (U80718), *Posidonia oceanica* (U80719), *Potamogeton crispus* (AB196847), *Potamogeton pusillus* (AB196950), *Ruppia cirrhosa* (JN113277), *Ruppia maritima* (U03729), *Ruppia megacarpa* (AB507891), *Stratiotes aloides* (U80709), *Stuckenia pectinata* (AB196953), *Symplocarpus foetidus* (L10247),

Syringodium filiforme (U03727), *Syringodium isoetifolium* (U80691), *Thalassia hemprichii* (U80710), *Thalassia testudinum* (U80711), *Thalassodendron ciliatum* (KF488498), *Triglochin bulbosa* (AM234996), *Triglochin maritima* (JX848473), *Vallisneria americana* (U03726), *Vallisneria spiralis* (U80712), *Zostera caespitosa* (AB125351), *Zostera capensis* (AM235166), *Zostera capricorni* (AY077963), *Zostera caulescens* (AB125350), *Zostera japonica* (AB125353), *Zostera marina* (AB125349), *Zostera mucronata* (U80732), *Zostera muelleri* (AY077962), *Zostera noltei* (U80733) and *Zostera tasmanica* (U80730). ***b***, list of the genes used in the phylogenetic studies included in the TimeTree analysis. References of the studies are also listed.

Supplementary Table 1. Indirect proxies of CO_2 concentrating mechanisms. Variables shown are the percentage of net photosynthetic rate inhibition after addition of acetazolamide (AZ, n = 9), ethoxyzolamide (EZ, n = 9), TRIS-buffer (TRIS, n = 10) and 4,40-diisothiocyanatostilbene-2,20-disulfonate (DIDS, n = 8); isotopic composition of ^{13}C from leaf biomass ($\delta^{13}C$, n = 6) and pH compensation point determined by pH-drift experiments (n = 9). Values are means ± s.e. In bold, mean values for the different environments. * Indicates statistically significant inhibition on the net photosynthetic rate ($P < 0.05$, Student's t-test or Mann-Whitney-Wilcoxon for non-parametric data). # Indicates significant differences between the net photosynthetic rate under the presence of AZ and EZ ($P < 0.05$, Student's t-test or Mann-Whitney-Wilcoxon for non-parametric data). Different small letters show significant differences among species, and capital letters show significant differences among environments ($P < 0.05$, one-way ANOVA followed by Duncan's test or Kruskal–Wallis test followed by Bonferroni correction for non-parametric data).

Species / environment	AZ	EZ	TRIS	DIDS	$\delta^{13}C$ (‰)	pH compensation point
Alisma lanceolatum	-	-	-	-	-30.78 ± 0.02 e	-
Triglochin maritima	-	-	-	-	-30.77 ± 0.05 e	-
Terrestrial average	-	-	-	-	**-30.77 ± 0.02 C**	-
Ceratophyllum demersum	36.8 ± 1.0 c*	68.8 ± 1.6 a*#	-13.9 ± 3.5 e	24.6 ± 1.9 a*	-21.57 ± 0.43 bc	10.6 ± 0.1 a
Vallisneria gigantea	56.6 ± 1.6 a*	72.0 ± 2.8 a*#	4.5 ± 3.0 d	10.5 ± 2.6 bc*	-26.17 ± 0.71 cd	10.3 ± 0.1 b
Freshwater average	**44.1 ± 2.4 A**	**69.8 ± 1.4 A**	**-4.34 ± 2.94 C**	**17.1 ± 2.4 A**	**-23.87 ± 0.86 B**	**10.4 ± 0.1 A**
Stuckenia pectinata	22.2 ± 1.9 d*	31.6 ± 2.4 cd*#	47.6 ± 1.8 c*	18.8 ± 2.1 ab*	-28.18 ± 0.25 d	9.8 ± 0.2 c
Ruppia cirrhosa	20.5 ± 1.5 d*	23.4 ± 2.8 d*	50.1 ± 2.1 bc*	4.1 ± 2.7 c	-11.56 ± 0.33 a	9.6 ± 0.1 c
Brackish water average	**21.4 ± 1.2 B**	**27.5 ± 2.0 C**	**49.05 ± 1.44 B**	**11.4 ± 2.4 A**	**-19.86 ± 1.92 B**	**9.7 ± 0.1 B**
Posidonia oceanica	47.1 ± 2.3 b*	44.5 ± 3.2 b*	45.6 ± 4.2 c*	15.7 ± 5.9 ab*	-16.67 ± 0.19 b	9.3 ± 0.1 d
Cymodocea nodosa	45.6 ± 1.8 b*	44.0 ± 4.5 b*	68.4 ± 3.9 a*	8.1 ± 5.8 bc	-11.13 ± 0.35 a	9.8 ± 0.0 c
Zostera marina	22.9 ± 2.6 d*	37.8 ± 4.1 bc*#	76.9 ± 1.9 a*	-10.0 ± 3.3 d	-12.28 ± 0.05 a	9.2 ± 0.1 d
Zostera noltii	26.6 ± 2.6 d*	35.3 ± 3.8 bc*#	58.7 ± 5.3 b*	-15.9 ± 3.7 d	-11.30 ± 0.16 a	9.6 ± 0.1 c
Seawater average	**37.2 ± 2.1 A**	**40.7 ± 2.0 B**	**65.65 ± 2.60 A**	**-2.4 ± 3.1 B**	**-13.16 ± 0.55 A**	**9.4 ± 0.1 C**

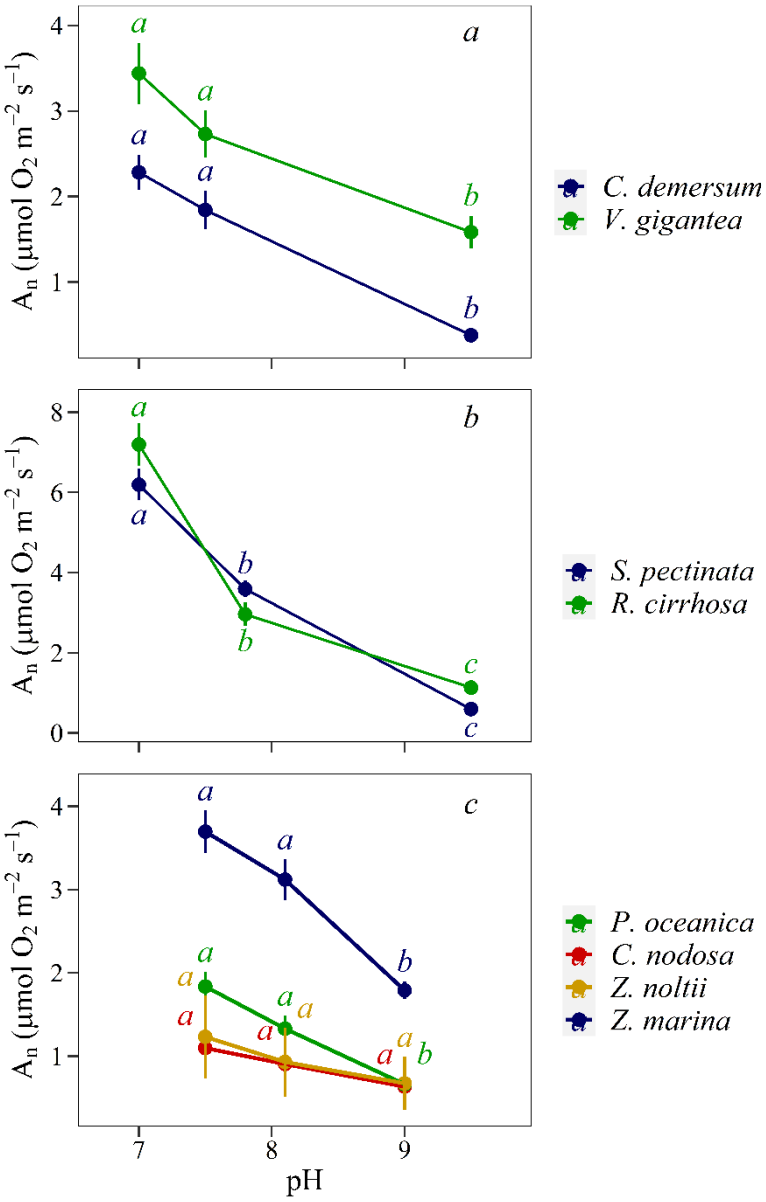

Supplementary Fig. 2. Net photosynthetic rates under different pH. ***a***, freshwater species; ***b***, brackish water species; ***c***, seawater species. Values are means ± s.e. Different letters show significant differences among net photosynthetic rates ($P < 0.05$, one-way ANOVA followed by Duncan's test or Kruskal–Wallis test followed by Bonferroni correction for non-parametric data, n = 8).

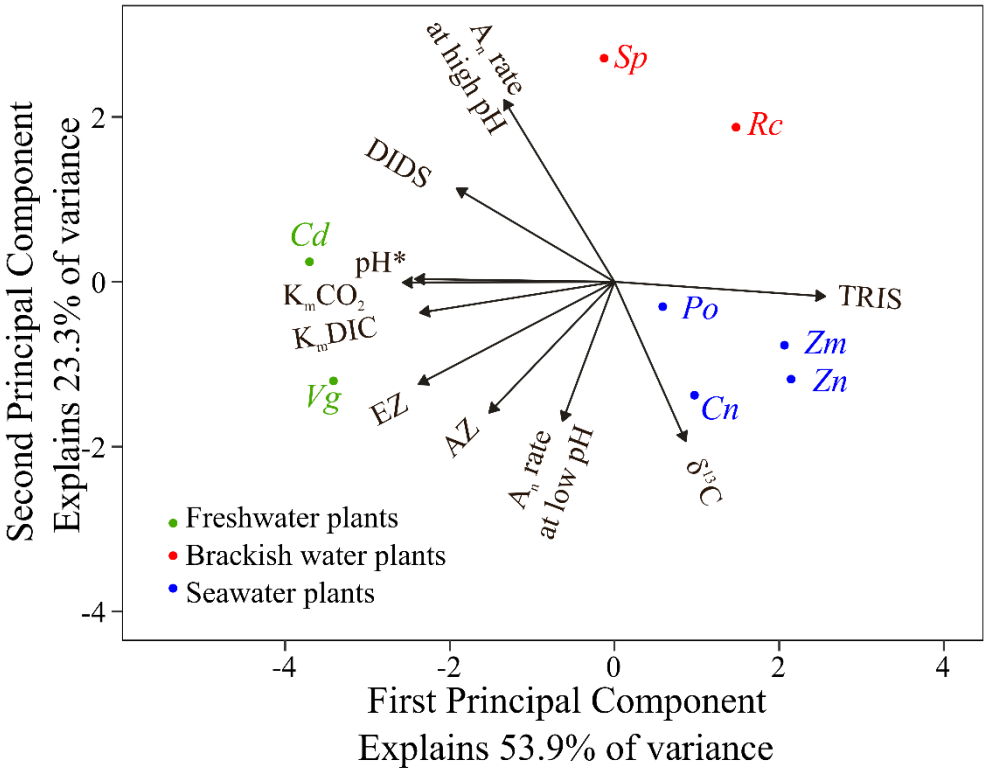

Supplementary Fig. 3. **Principal Component Analysis of the CO_2 concentrating mechanism proxies analysed**. Parameters included are: isotopic discrimination of ^{13}C of leaf biomass ($\delta^{13}C$), pH compensation point determined by pH-drift assay (pH*), *in vivo* photosynthetic semi-saturation constant for CO_2 (K_m CO_2) and for dissolved inorganic carbon (K_m DIC), percentage of the net photosynthetic rate inhibition after addition of acetazolamide (AZ), ethoxyzolamide (EZ), TRIS-buffer (TRIS) and 4,40-diisothiocyanatostilbene-2,20-disulfonate (DIDS), and the percentage of the net photosynthetic rate variation at pH 9-9.5 (A_n rate at high pH) and at pH 7-7.5 (A_n rate at low pH) relative to water environmental pH (pH ~8).

Supplementary Table 2. **Leaf N and Rubisco content.** Variables shown are percentage of Rubisco per total soluble protein (TSP; n = 8), leaf nitrogen content (n = 5) and maximum net photosynthetic rate *in vivo* ($A_{n\ max}$, n = 5 - 8) obtained from photosynthesis-CO_2 curves. Values are means ± s.e. In bold are the mean values for the different environments. Different small letters show significant differences among species, and capital letters show significant differences among environments ($P < 0.05$, one-way ANOVA followed by Duncan's test or Kruskal–Wallis test followed by Bonferroni correction for non-parametric data).

	Rubisco (% of TSP)	**N (g m^{-2})**	**$A_{n\ max}$ *in vivo* (µmol O_2 or CO_2 m^{-2} s^{-1})**
Alisma lanceolatum	13.8 ± 2.0 ab	1.45 ± 0.01 a	36.09 ± 2.43 a
Triglochin maritima	20.5 ± 2.0 a	1.07 ± 0.01 ab	45.69 ± 2.11 a
Terrestrial average	**17.67 ± 1.89 A**	**1.26 ± 0.06 A**	**40.89 ± 2.20 A**
Ceratophyllum demersum	6.2 ± 0.4 ab	0.64 ± 0.05 cd	2.91 ± 0.35 bc
Vallisneria gigantea	3.7 ± 0.4 c	0.69 ± 0.02 c	2.33 ± 0.18 cd
Freshwater average	**4.68 ± 0.41 B**	**0.67 ± 0.02 B**	**2.68 ± 0.23 C**
Stuckenia pectinata	4.0 ± 0.4 bc	0.81 ± 0.01 b	4.91 ± 0.54 ab
Ruppia cirrhosa	4.0 ± 0.3 bc	0.7 ± 0.01 c	5.47 ± 0.71 ab
Brackish water average	**4.02 ± 0.26 B**	**0.76 ± 0.02 B**	**5.21 ± 0.45 B**
Posidonia oceanica	3.0 ± 0.4 c	0.29 ± 0.01 f	1.83 ± 0.10 d
Cymodocea nodosa	3.3 ± 0.2 c	0.51 ± 0.02 de	1.61 ± 0.25 d
Zostera marina	3.9 ± 0.3 bc	0.28 ± 0 ef	2.36 ± 0.12 cd
Zostera noltii	3.8 ± 0.3 c	0.25 ± 0.01 f	1.54 ± 0.35 d
Seawater average	**3.55 ± 0.18 B**	**0.33 ± 0.02 C**	**1.83 ± 0.12 D**

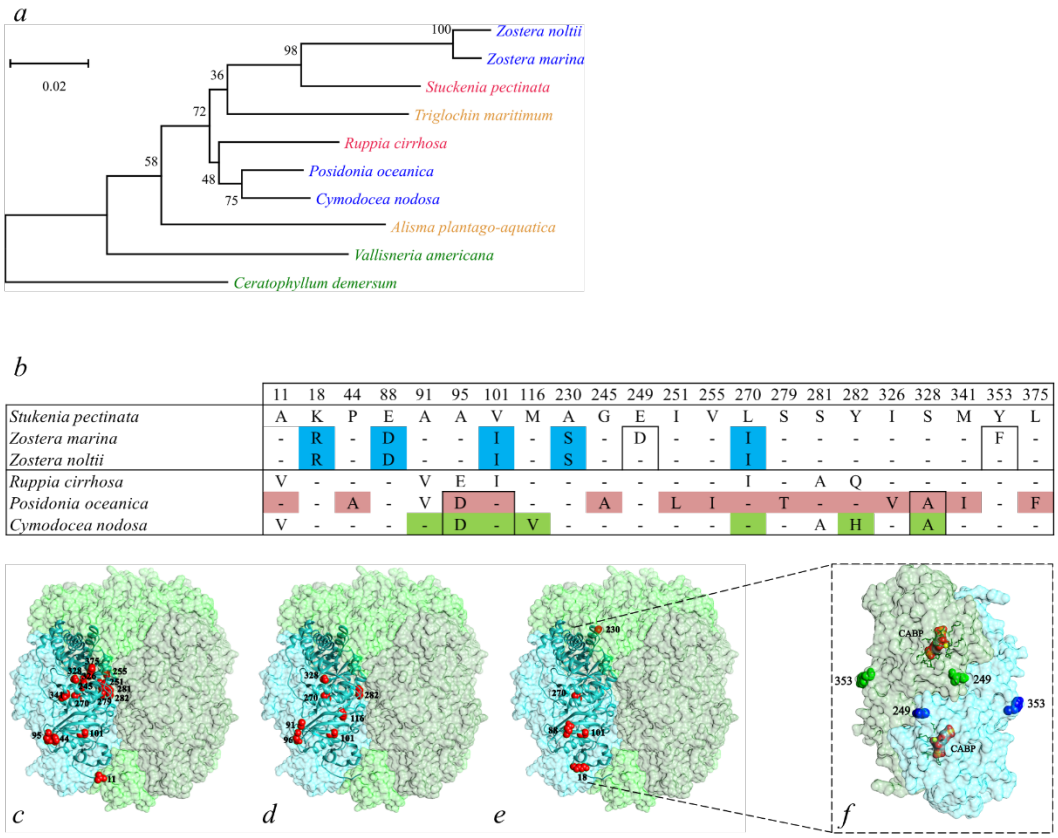

Supplementary Fig. 4. *rbc*L and amino acid Rubisco large subunit analyses. *a*, Maximum likelihood tree inferred from the *rbc*L of the species selected in this study**.** Bootstrap values (from 1000 replicates) are indicated at the nodes. Colour names indicate the environment of the species: blue are seagrasses species, red are brackish water species, green are freshwater species and orange terrestrial species. ***b***, Alignment of the *rbc*L amino acid sequences from the species belonging to the two main branches identified in the previous maximum likelihood tree containing the analysed seagrasses. In blue, amino acid changes among *Stuckenia pectinata*, and *Zostera* species; in red, amino acid changes between *Ruppia cirrhosa* and *Posidonia oceanica*; in green, amino acid changes between *Ruppia cirrhosa* and *Cymodocea nodosa*. Amino acids in boxes denote differences between *Z. noltii* and *Z. marina* and amino acid changes shared by *C. nodosa* and *P. oceanica*. ***c***, localisation of variable amino acid sites between *R. cirrhosa* and *P. oceanica*. ***d***, localisation of variable amino acid sites between *R. cirrhosa* and *C. nodosa.* ***e***, localisation of variable amino acid sites between *Stuckenia pectinata* and *Zostera* species. ***f***, localisation of variable amino acid sites between *Z. noltii* and *Z. marina*. Two L-subunits forming a functional dimer are highlighted in green and cyan in all Rubisco structures showed. Rubisco L-subunit residues are presented on the structure of spinach Rubisco (1UPM) using UCSF Chimera V1.12.

Note: The large phylogenetic distance among the species made difficult to relate the particularities of Rubisco catalytic properties of seagrasses to specific amino acid changes. However, the two congeneric *Zostera* species included in the study only differed at positions 249 and 353 of the Rubisco large subunit sequence (Supplementary Fig. 4f),

which coincide with a significantly lower $S_{c/o}$ in *Z. noltii* compared with *Z. marina* (Table 1).

Supplementary Table 3. Description of the amino acid changes detected in Supplementary Fig. 4b based on literature

Amino Acid	Domain	Secondary structure	Interaction	References
A 11	N-terminal	-	-	Knight et al.[3]
K 18	N-terminal	-	-	Knight et al.[3]
P 44	N-terminal	βB	Amino acid residue in the core of the N-terminal domain of the large subunit	Knight et al.[3]
E 88	N-terminal	βC	-	Knight et al.[3]
A 91	N-terminal	-	Close to functional amino acid 94	Sharwoood et al.[4]
A 95	N-terminal	-	Close to functional amino acid 94	Sharwoood et al.[4]
V 101	N-terminal	βD	Amino acid residue in the core of the N-terminal domain of the large subunit	Knight et al.[3]
M 116	N-terminal	αC	Amino acid residue in the core between the N-terminal and the C-terminal domain of the large subunit	Knight et al.[3]
A 230	C-terminal	α2	Amino acid residue at the interface between the small subunit and the large subunit. It forms hydrogen bonds between the small subunit and the large subunit	Knight et al.[3]
G 245	C-terminal	-	Residue at the interface between the C-terminal domain of one subunit and the N-terminal domain of the second subunit in the L2 dimer	Knight et al.[3]
E 249	C-terminal	α3	-	Knight et al.[3]
I 251	C-terminal	α3	-	Knight et al.[3]
V 255	C-terminal	α3	-	Knight et al.[3]
L 270	C-terminal	-	-	Knight et al.[3]
S 279	C-terminal	α4	Residue at the interface between the C-terminal domains of the 2 subunits in the L2 dimer. It forms hydrogen bonds between the 2 C-terminal domains	Knight et al.[3]
S 281	C-terminal	α4	-	Knight et al.[3]
Y 282	C-terminal	α4	-	Knight et al.[3]
I 326	C-terminal	β6	Amino acid residue in the circular core between helices and strands in the α/β-barrel in the large subunit. Close to Rubisco active site residues.	Knight et al.[3]
S 328	C-terminal	-	Amino acid residue in the circular core between helices and strands in the α/β-barrel in the large subunit. Close to Rubisco active site residues. Close to Rubisco active site. A reported functional amino acid to be responsible for Sc/o improvments	Knight et al.[3], Sharwoood et al.[4], Galmés et al.[5]
M 341	C-terminal	α6	Located closely to active site residue E 340	Hartman & Harpel[6]
Y 353	C-terminal	βG	-	Knight et al.[3]
L 375	C-terminal	β7	Located closely to active site residue A 378	Hartman & Harpel[6]

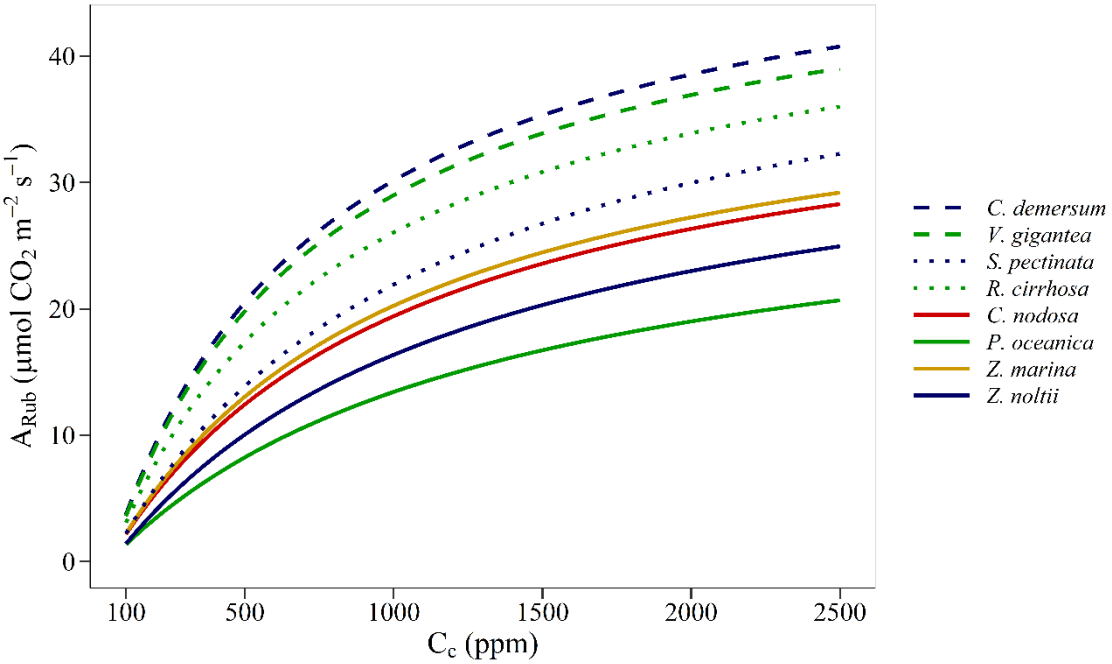

Supplementary Fig. 5. Modelled Rubisco gross assimilation rate (A_{Rub}) for the analysed aquatic species. Solid line, seagrasses; dotted line, brackish water species; dashed line, freshwater species. The photosynthesis model of Farquhar et al.[7] was used to model A_{Rub} at the different concentrations of chloroplastic CO_2 (C_c). This modelling exercise was done assuming CO_2 assimilation rates under saturating light conditions and Rubisco content standardized to 1 g m^{-2}.

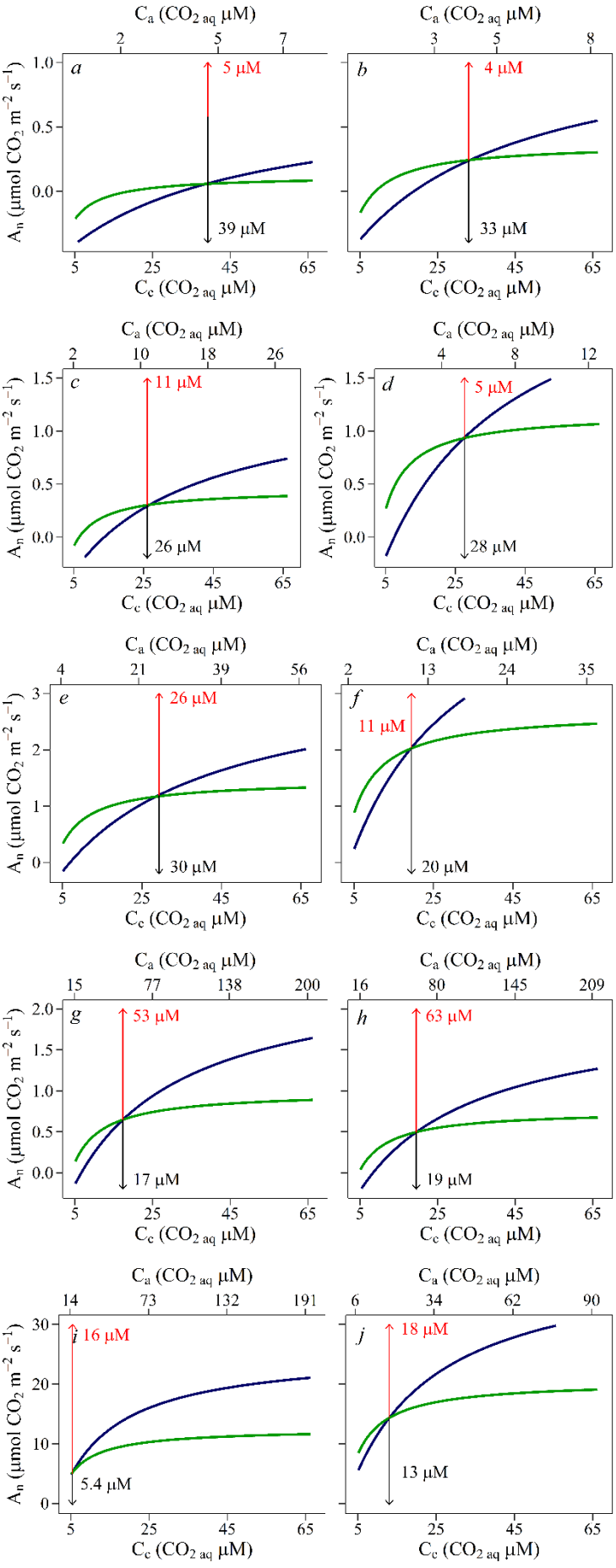
a
5 µM
39 µM
b
4 µM
33 µM
c
11 µM
26 µM
d
5 µM
28 µM
e
26 µM
30 µM
f
11 µM
20 µM
g
53 µM
17 µM
h
63 µM
19 µM
i
16 µM
5.4 µM
j
18 µM
13 µM
Ca (CO2 aq µM)
Cc (CO2 aq µM)
An (µmol CO2 m−2 s−1)

Supplementary Fig. 6. Modelled leaf net photosynthetic rate as a function of chloroplastic CO_2 (C_c) using equations of the photosynthetic C_3 model of Farquhar et al.[7] and the Rubisco kinetic data for each species. ***a***, *P. oceanica*; ***b***, *Z. noltii*; ***c***, *Z. marina*; ***d***, *C. nodosa*; ***e***, *S. pectinata*; ***f***, *R.cirrhosa*; ***g***, *C. demersum*; ***h***, *V. gigantea*; ***i***, *T. maritima*; ***j***, *A. lanceolatum*. In blue is respresented the Rubisco-limited rate of CO_2 assimilation (A_c) and in green, the electron-transport limited rate of CO_2 assimilation (A_j). The equivalent extracellular CO_2 concentration (C_a) is shown in the upper *x* axis.

Supplementary Table 4. Interannual variability of the physicochemical variables from the different aquatic environments.

Environment	Species	Salinity (psu) [a]	pH [b]	Alkalinity ($\mu eq\ l^{-1}$) [c]	DIC [d] (μM)	HCO_3^- (μM)	CO_3^{2-} (μM)	CO_2 (μM)
River/lake (Freshwater)	*C. demersum* *V. gigantea*	3.3 - 10.8	7.1 - 10.5	2900 - 5900	1450 - 6818	124 - 5873	1.326 - 13	0 - 931
Coastal marsh (Brackish water)	*S. pectinata* *R. cirrhosa*	5.9 - 36.9	7.4 - 8.0	1000 - 3600	869 - 3827	797 - 3555	22 – 64	7 - 250
Sea (Seawater)	*P. oceanina* *C. nodosa* *Z. marina* *Z. noltii*	37.0 - 38.2	8.0 - 8.1	~ 2300	2029 -2089	1824 - 1916	155 – 191	14 – 18

[a], salinity values of aquatic environments extracted from Martínez Taberner et al.[8] and Puigserver et al.[9]. [b], pH values of aquatic environments extracted from Joesoef et al.[10], Maberly and Gontero[11] and Martínez Taberner et al. [8]. [c], values of alkalinity extracted from Maberly and Gontero[11], Martínez Taberner et al. [8], Oliveira et al.[12] and Puigserver et al.[9]. [d], DIC, HCO_3^- CO_3^{2-} and CO_2 concentrations were calculated with the software CO2sys V2.2

Supplementary Table 5. Measured physicochemical variables at 25ºC of the water collected from the species respective environments. Isotopic discrimination of DIC from the aquatic environment ($\delta^{13}C_{DIC}$, n = 4, represented mean ± uncertainty of measurement). DIC, HCO_3^- CO_3^{2-} and CO_2 concentrations were calculated with the software CO2sys V2.2.

Environment	Species	Salinity (psu)	pH	Alkalinity (µeq l^{-1})	DIC (µM)	HCO_3^- (µM)	CO_3^{2-} (µM)	CO_2 (µM)	$\delta^{13}C_{DIC}$ (‰)
Freshwater	*C. demersum*	0.37	7.5	3750	4048	3734	8	306	-0.1 ± 0.18
Freshwater	*V. gigantea*	0.37	7.5	3750	4048	3734	8	306	-0.1 ± 0.18
Brackish water	*S. pectinata*	7.0	7.8	5995	6048	5795	97	156	-12.0 ± 0.07
Brackish water	*R. cirrhosa*	10.0	8.0	6549	6432	6139	199	94	-7.9 ± 0.08
Seawater	*P. oceanina*	37.0	8.15	2627	2308	2059	235	14	-0.5 ± 0.05
Seawater	*C. nodosa*	37.0	8.15	2627	2308	2059	235	14	-0.5 ± 0.05
Seawater	*Z. marina*	36.5	8.05	2678	2420	2203	197	19	-0.5 ± 0.05
Seawater	*Z. noltii*	37.0	8.15	2627	2308	2059	235	14	-0.5 ± 0.05

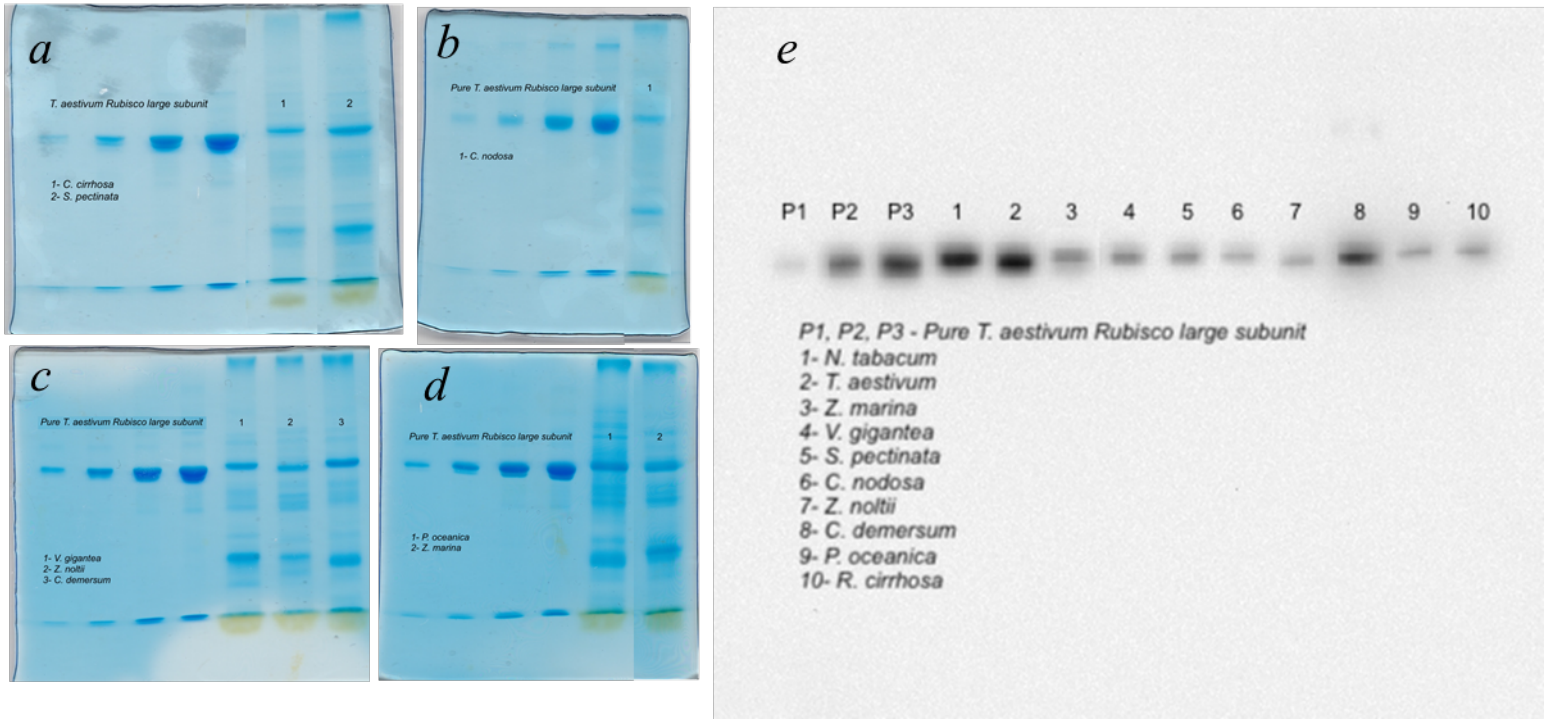

Supplementary Fig. 7. Examples of Coomassie stain SDS-PAGE blots (*a-d*), and inmunoblots (*e*) used to confirm the Rubisco content determined by ^{14}C-CABP binding sites in the analysed aquatic species. Pure *Triticum aestivum* Rubisco large subunit was used as standard for the Coomassie stain SDS-PAGE blots.

References

1. Hedges, S. B., Marin, J., Suleski, M., Paymer, M. & Kumar, S. Tree of life reveals clock-like speciation and diversification. *Mol. Biol. Evol.* **32**, 835–845 (2015).

2. Kumar, S., Stecher, G., Suleski, M. & Hedges, S. B. TimeTree: A Resource for Timelines, Timetrees, and Divergence Times. *Mol. Biol. Evol.* **34**, 1812–1819 (2017).

3. Knight, S., Andersson, I. & Brändén, C. I. Crystallographic analysis of ribulose 1,5-bisphosphate carboxylase from spinach at 2·4 Å resolution. Subunit interactions and active site. *J. Mol. Biol.* **215**, 113–160 (1990).

4. Sharwood, R. E., Ghannoum, O., Kapralov, M. V., Gunn, L. H. & Whitney, S. M. Temperature responses of Rubisco from Paniceae grasses provide opportunities for improving C_3 photosynthesis. *Nat. Plants* **2**, 1–9 (2016).

5. Galmés, J. *et al.* Environmentally driven evolution of Rubisco and improved photosynthesis and growth within the C_3 genus *Limonium* (Plumbaginaceae). *New Phytol.* **203**, 989–999 (2014).

6. Hartman, F. C. & Harpel, M. R. Structure, function, regulation, and assembly of D-ribulose-1,5-bisphosphate carboxylase/oxygenase. *Annu. Rev. Biochem.* **63**, 197–234 (1994).

7. Farquhar, G., Caemmerer, S. Von & Berry, J. A. A biochemical model of photosynthetic CO_2 assimilation in leaves of C_3 species. *Planta* **90**, 78–90 (1980).

8. Martínez Taberner, A., Moyá, G. & Ramón, G. Aportación al conocimiento de la mineralización de las aguas de la albufera de Alcúdia (Mallorca). intento de clasificación. *Bolletí la Soc. d'Història Nat. les Balear.* **29**, 87–108 (1985).

9. Puigserver, M., Ramon, G., Moya, G. & Martínez-Taberner, A. Planktonic chlorophyll *a* and eutrophication in two Mediterranean littoral systems (Mallorca Island, Spain). *Hydrobiologia* **1**, 475–476 (2002).

10. Joesoef, A., Kirchman, D. L., Sommerfield, C. K. & Cai, W.-J. Seasonal variability of the inorganic carbon system in a large coastal plain estuary. *Biogeosciences* **14**, 4949–4963 (2017).

11. Maberly, S. C. & Gontero, B. Ecological imperatives for aquatic CO_2-concentrating mechanisms. *J. Exp. Bot.* **68**, 3797–3814 (2017).

12. Oliveira, A. P., Cabeçadas, G. & Mateus, M. D. Inorganic carbon distribution and CO_2 fluxes in a large European estuary (Tagus, Portugal). *Sci. Rep.* **7**, 1–14 (2017).